Research Article

Coexistence of the Bandcount-Adding and Bandcount-Increment Scenarios

Viktor Avrutin, Michael Schanz, and Björn Schenke

IPVS, University of Stuttgart, Universitätstrasse 38, 70569 Stuttgart, Germany

Correspondence should be addressed to Björn Schenke, bjoern.schenke@ipvs.uni-stuttgart.de

We investigate the structure of the chaotic domain of a specific one-dimensional piecewise linear map with one discontinuity. In this system, the region of "robust" chaos is embedded between two periodic domains. One of them is organized by the period-adding scenario whereas the other one by the period-increment scenario with coexisting attractors. In the chaotic domain, the influence of both adjacent periodic domains leads to the coexistence of the recently discovered bandcount adding and bandcount-increment scenarios. In this work, we focus on the explanation of the overall structure of the chaotic domain and a description of the bandcount adding and bandcount increment scenarios.

1. Introduction

Piecewise smooth maps are in the meanwhile known to be appropriate models of many dynamical processes in science and technology as mentioned already in textbooks on this topic [1–4]. Standard examples mentioned in these books are from the fields of electronics, mechatronics, and mechanics like power converters, impacting systems, systems with suspensions, gears, transmissions, or ball bearings. Additionally to these usual applications further examples range from systems in micro- and nanotechnology, in particular piezoelectric energy harvesting devices and devices using piezoelectric or other micro-machined actuators [5, 6] to generate movement or propulsion in a very precise manner, up to several models [7–9] of the famous Fermi accelerator [10] as a possible explanation of high-energetic cosmic radiation. Furthermore they occur naturally as one- or two-dimensional Poincaré maps of corresponding time continuous flows [11–13]. The inherent state space reduction allows in many cases a much more efficient investigation of the dynamic behavior than the original flow. In this work we investigate a specific

one-dimensional piecewise linear map derived from the "canonical form" [14] of one-dimensional piecewise linear maps with a single discontinuity. Since the pioneer works [15, 16], it is known that the system

$$
x_{n+1} = \begin{cases} f_\ell(x_n) = ax_n + \mu, & \text{if } x_n < 0, \\ f_r(x_n) = bx_n + \mu + l, & \text{if } x_n > 0 \end{cases} \tag{1.1}
$$

represents some kind of discontinuous canonical form for border-collision bifurcations. It can be shown [17] that for the dynamic behavior of this system the exact value of the parameter l is not significant but only the sign of l, so there are three characteristic cases $l < 0$, $l > 0$ and $l = 0$. The first two cases represent discontinuous maps having a positive or negative jump, respectively. The third case represents the skew tent map, a continuous map with different slopes of the system function on the left- and right-hand side of the point of discontinuity. This map was investigated since the pioneer works by Maistrenko et al. [18, 19] and by many authors (see, e.g., references in [3, 4]).

The case of the negative jump has already been studied in several works, both in the regular (periodic or aperiodic but not chaotic) and in the chaotic domain. In these works, it was discovered that an extended part of the regular domain of the negative jump case is structured by a bifurcation scenario denoted as period increment scenario with coexisting attractors while the adjacent chaotic domain is structured by the bandcount-increment bifurcation scenario [20–22]. The first scenario is formed by border collision bifurcations where an attracting periodic orbit collides with the point of discontinuity and disappears, so that after the bifurcation the system evolves to a different attractor. By contrast, the second scenario is formed by crisis bifurcations. Here, before and after the bifurcation the system shows chaotic behavior. However, at the bifurcation point the structure of the chaotic attractor, especially the number of bands (connected components, also known as cyclic chaotic intervals) changes. The remaining part of the periodic domain of the negative jump case was found to be structured by the period adding bifurcation scenario and the adjacent chaotic domain by the bandcount-adding bifurcation scenario [17, 23].

To avoid misunderstandings, note that the notation "period adding" is used in the literature for different bifurcation scenarios. In this work we use a notation based on the fact that there exists a bifurcation structure where the periods of subsequent periodic orbits form an arithmetic progression: $p_{n+1} = p_n + \Delta p = p_0 + n\Delta p$. It is known that three different cases are possible. In the first case the existence regions of the orbits with periods p_n and p_{n+1} overlap (see Figure 1(a)) and we denote this bifurcation scenario as period increment scenario with coexistence of attractors. In the second case the existence regions of the orbits with periods p_n and p_{n+1} adjoin each other without overlapping and without a gap between them. Accordingly, we denote this situation as pure period increment scenario. In the last case the situation is more complex. There is a gap between the existence regions of two subsequent periodic orbits and the behavior in these gaps can be either periodic or chaotic. In the first case one well-known situation is given by the self-similar Farey-tree like bifurcation structure where between the existence regions of two periodic orbits with periods p_n and p_{n+1} there exists a region with period $p_n + p_{n+1}$ and so on ad infinitum (see Figure 1(b)). In the following we denote this scenario as period adding scenario.

(a)

(b)
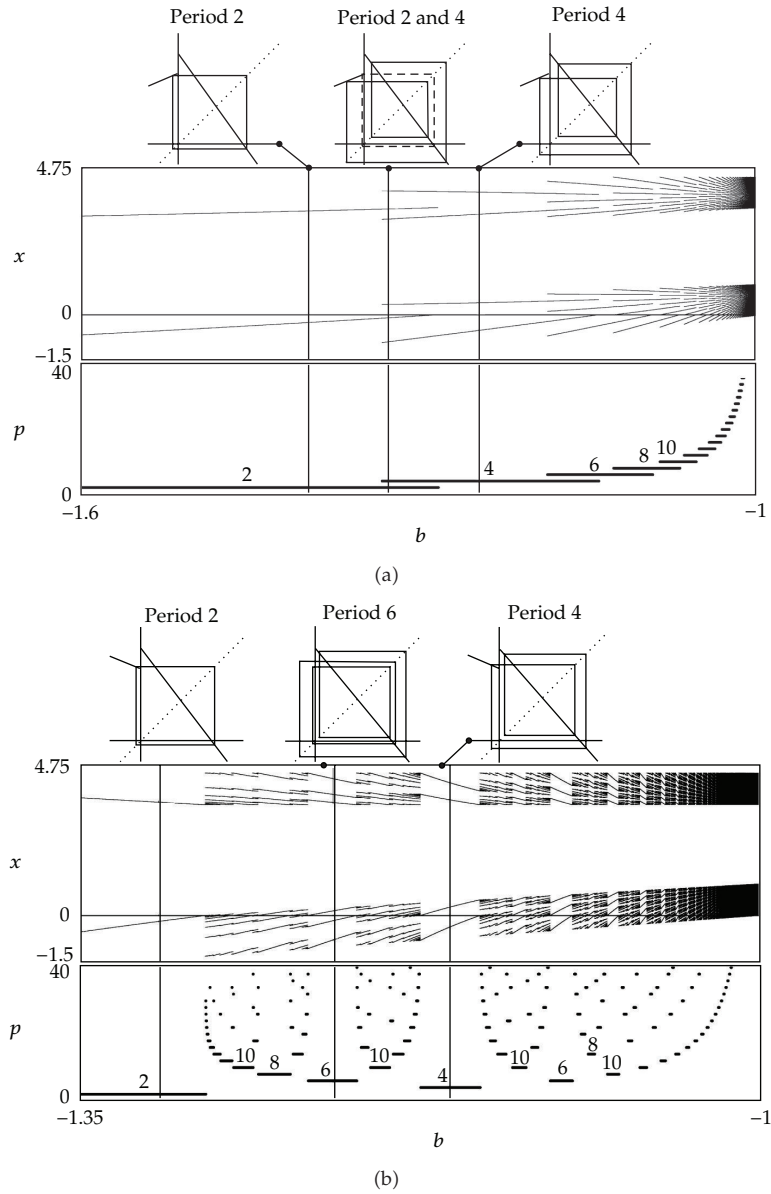
Figure 1: The period increment scenario with coexisting attractors (a) and the period adding scenario (b) in map (1.3). For each scenario three sketches of the map, a bifurcation diagram and a period diagram are shown. Parameter values are: $a = 0.42$, $\mu = 3.5$ (a) and $a = -0.42$, $\mu = 3.5$ (b). Their locations are shown in Figure 2 with gray lines marked with "D" and "E".

In this work we study the case of the positive jump, which can be transformed into a standard form, which simplifies analysis. For any $l > 0$ the transformation

$$(x, a, b, \mu) \longmapsto (lx', a, b, l\mu') \tag{1.2}$$

leads us (by dropping the prime) to the map

$$x_{n+1} = \begin{cases} f_\ell(x_n) = ax_n + \mu, & \text{if } x_n < 0, \\ f_r(x_n) = bx_n + \mu + 1, & \text{if } x_n > 0, \end{cases} \tag{1.3}$$

which we will investigate in the following and which can be seen as a canonical form of discontinuous linear maps with a positive jump.

The domain of regular dynamics of map (1.3) was investigated in [24]. In this work it was shown that this system has a domain of "robust" chaos (in the sense of Banerjee et al. [25]) embedded between the two regular domains. However, the structure of the chaotic domain of this system was not investigated.

The first results related to bifurcations occurring in the chaotic domain are going back to the works by Mira and Gumowski [26–30]. Already in the 60s they discovered a large class of bifurcations, called contact bifurcations, which result from contacts of two invariant sets. These bifurcations were later rediscovered by Grebogi et al. in the beginning of the 80s [31, 32] and denoted as crises bifurcations. Obviously, if one of the involved invariant sets is given by a chaotic attractor, then a contact bifurcation represents a crisis in the sense mentioned above, so the crises represent a subclass of contact bifurcations. Since then crises bifurcations were observed and investigated in several application fields [33–38]. However, the bifurcation structure formed only by crises bifurcations and organizing the robust chaotic domain are barely investigated so far.

Examples of such bifurcation structures were recently reported in [20–23]. There it is shown, that the structure of the chaotic domain is strongly influenced by the structure of the adjacent periodic domain. If this adjacent periodic domain is structured by the period adding scenario in the sense mentioned above, then the robust chaotic domain is structured by the bandcount-adding scenario. By contrast, in the case of an adjacent periodic increment scenario with coexistence of attractors the chaotic domain is structured by the bandcount-increment scenario.

By contrast to the situations investigated in the cited works where the domain of robust chaos is located between regular and divergent domains, the results shown in [24] imply that in map (1.3) the chaotic domain is sandwiched between two regular domains, one of them organized by the period adding scenario and the other one by the periodic increment scenario with coexistence of attractors. Therefore, one can assume that in this case the chaotic domain is organized by both, bandcount-adding and bandcount-increment scenarios. This fact will be demonstrated in the paper.

Furthermore, the question arises whether there is any interaction between the scenarios. Is it possible, that the unstable periodic orbits which induce one of the bandcount scenarios lead to changes in the other bandcount scenario? Can the scenarios overlap? Is the complete chaotic domain between period adding and period increment covered by their bandcount counterparts, or is there a region which is structured by neither of them? Also, apart from any possible interaction, it is interesting to see if there are significant differences in the bandcount scenarios as they occur in system (1.3), and the previously discovered ones. In this work, we examine in which regions in parameter space the bandcount-adding and increment scenarios exist and we examine each scenario to determine if any interaction takes place.

This work is structured as follows. After this introduction, we explain in Section 2 symbolic sequences and kneading orbits, which are two important technical concepts

required for the understanding of this work. In Section 3 we describe the investigated region in parameter space and the big bang bifurcations structuring this region. In Section 4 we summarize the structure of the periodic domain by explaining in short the period adding and the period increment scenarios. In Section 5 we give an overview over the structure of the chaotic domain. It consists of three different regions, Q^{add}, Q^{inc}, and Q^1. The boundaries separating these three regions are explained in Section 5.1 and their properties are described in Section 5.2, whereas the following sections describe the bifurcation structure inside the regions Q^{add} and Q^{inc}. In Section 6, the bandcount-adding region Q^{add} is described, whereby Section 6.1 is devoted to the overall bandcount-adding structure and Section 6.2 to its nested-substructures. The boundary between period adding and bandcount-adding shows some interesting behavior, which is described in Section 7. Finally, in Section 8, we give an overview over the region Q^{inc} and the bandcount increment structure located therein.

2. Symbolic Sequences and Kneading Orbits

Important for all descriptions that involve periodic orbits is the concept of symbolic sequences [39]. A symbolic sequence is a sequence of the letters $\mathcal{L}$ and $\mathcal{R}$, each representing a single point of an orbit. $\mathcal{L}$ stands for a point $x < 0$ and $\mathcal{R}$ for a point $x > 0$. Note that when dealing with periodic orbits, only the symbols necessary for describing one period will be written and hence the symbolic sequences are shift-invariant. We denote a periodic orbit which corresponds to the symbolic sequence σ as O_σ.

The chaotic domain of map (1.1) in the case $l = +1$ is organized in a similar way as in the above-mentioned case $l = -1$. This means it is structured by interior and band-merging crises. Note that we refer to the band-merging crisis as "crisis", even though there is no discontinuous change in the overall size of the attractor. Instead, there is a discontinuous change in the number of bands of the attractor and consequently also in its topological structure.

Both interior and merging crisis share the property that they can be determined by calculating the intersection of a point of the colliding unstable periodic orbit with the boundary of the chaotic attractor. For that, one has to determine the boundary of a chaotic attractor. This is done using kneading theory by following up kneading orbits, that means the forward iterates or itineraries of the critical points. We remark that this idea is going back to the works by Gumowski and Mira [28, 29]. Already in 1977 they recognized that the boundaries of chaotic attractors in 2D maps are given by itineraries of some critical lines (*lignes critiques*). For details we refer to [40]. Of course, when dealing with 1D maps, these critical lines represent critical points and their itineraries define the kneading orbits.

Following this idea, a kneading orbit is an orbit started at a critical value of the system function, which is given for system (1.3) by $x = 0$. It has the property of jumping between the maxima and minima of the bands of a chaotic attractor, until it reaches a specific length, after which it leaves the boundaries of the attractor. Because system (1.3) is discontinuous at the critical point $x = 0$, there exist two different kneading orbits, one beginning with $f_l(0)$ and the other beginning with $f_r(0)$.

For the kneading orbits we use the following compact notation. A point of a kneading orbit given by $f_a \circ f_b \circ f_c \circ f_d \circ \cdots \circ f_z(0)$, with $a, b, c, d, z \in \{r/\ell\}$, is written as $x^{ko}_{z\cdots dcba}$. This means that the sequence of iteration steps leading to this point starts with $f_z(0)$ and ends with $f_a(x^{ko}_{z\cdots dcb})$. This is similar to the symbolic sequences used for periodic orbits. Note that the sequences used for kneading orbits are not shift-invariant.

3. Investigated Parameter Space Region and Big Bang Bifurcations

The periodic dynamics of system (1.3) is investigated in [24]. It is shown in this work that the periodic domain of system (1.3) is organized by four codimension-3 big bang bifurcations. A big bang bifurcation point in a n-dimensional parameter space is an intersection point of infinitely many $(n-1)$-dimensional bifurcation surfaces. The periods and symbolic sequences of the periodic orbits existing between these bifurcation surfaces are organized by a rule specific to the type of the big bang bifurcation. A big bang bifurcation point has an influence region which is composed of the union of the existence regions of all its periodic orbits. So by determining the location and type of a big bang bifurcation point, the structure of its complete influence region can be determined as well. The codimension-3 big bang bifurcation points found in system (1.3) are of the specific type initially described in [41]. A bifurcation point B of this type possesses an extended influence region $\Omega(B)$ in the 3D parameter space, which is organized by two manifolds, a 2D manifold $\mathcal{M}^{2D}(B)$ and a 1D manifold $\mathcal{M}^{1D}(B)$. Within the influence region $\Omega(B)$ the bifurcation structure above the 2D manifold $\mathcal{M}^{2D}(B)$ is given by the period adding phenomenon. We denote the corresponding part of $\Omega(B)$ by $\Omega^{add}(B)$. In the 2D manifold the structure is given by the pure period increment phenomenon and below $\mathcal{M}^{2D}(B)$ by the period increment phenomenon with coexisting attractors. The part of $\Omega(B)$ organized by the period increment phenomenon with coexisting attractors is denoted in the following by $\Omega^{inc}(B)$. Hereby the terms "above" and "below" refer to the direction of the 1D manifold $\mathcal{M}^{1D}(B)$.

An inherent property of system (1.3), which is reflected in the structure of its parameter space, is given by the symmetry

$$f(a, b, \mu, x) = -f(b, a, -(\mu + 1), -x). \tag{3.1}$$

This symmetry implies that the bifurcations occur in this system pairwise and generate identical structures in the parts of the parameter space, which can be mapped onto each other by (3.1). Therefore, it is sufficient to consider only two of the codimension-3 big bang bifurcations organizing the 3D parameter space of system (1.3).

In [24] it is shown that the region in the parameter space given by

$$P = \{(a, b, \mu) \mid |a| < 1, \ b < -1, \ \mu \geq 0\} \tag{3.2}$$

is organized by two codimension-3 big bang bifurcations occurring at the points

$$B_1 = (0, -1, 0), \qquad B_2 = (0, -1, \infty). \tag{3.3}$$

The two other codimension-3 big bang bifurcations occur at the points

$$B_1' = (-1, 0, -1), \qquad B_2' = (-1, 0, -\infty) \tag{3.4}$$

and organize the part of the parameter space symmetric to P with respect to the symmetry (3.1). If $|a| > 1$, there exist no stable periodic orbits for all values of b and μ in P. As we concern ourselves in this work with the part of the parameter space which is located between

(a) $a < 0$

(b) $a = 0$

(c) $a > 0$
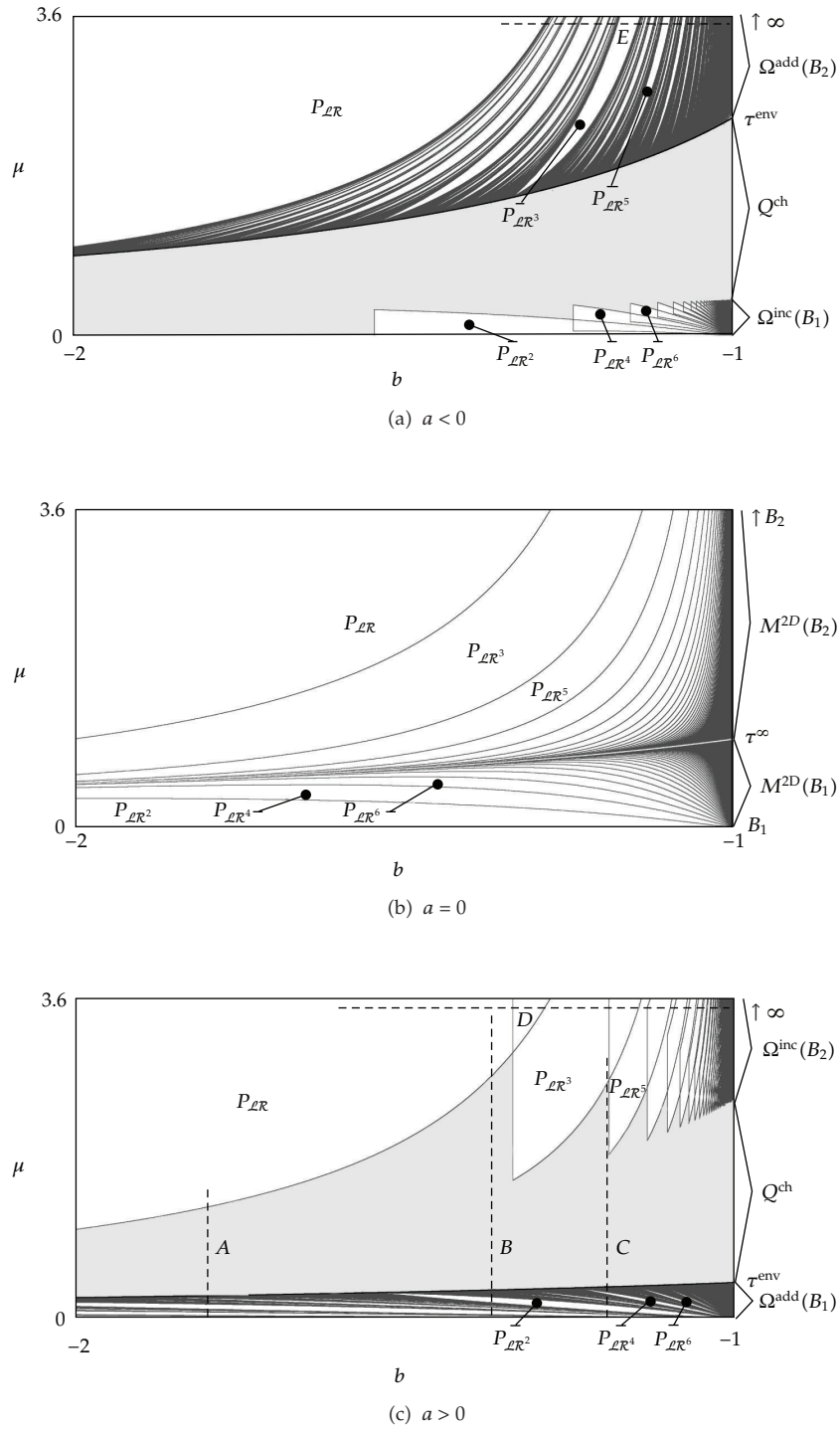
Figure 2: Numerically calculated bifurcation structures in the (b, μ)-plane for $a = -0.42$ (a), $a = 0$ (b), $a = 0.42$ (c), and $b = -2.0 \cdots -1.0$, $\mu = 0 \cdots 3.6$. The gray areas in (a) and (c) mark the chaotic domain Q^{ch}. The dashed lines in (a) and (c) show the locations of the bifurcation scenarios, shown in Figures 1, 3, and 5.

(a)

(b)
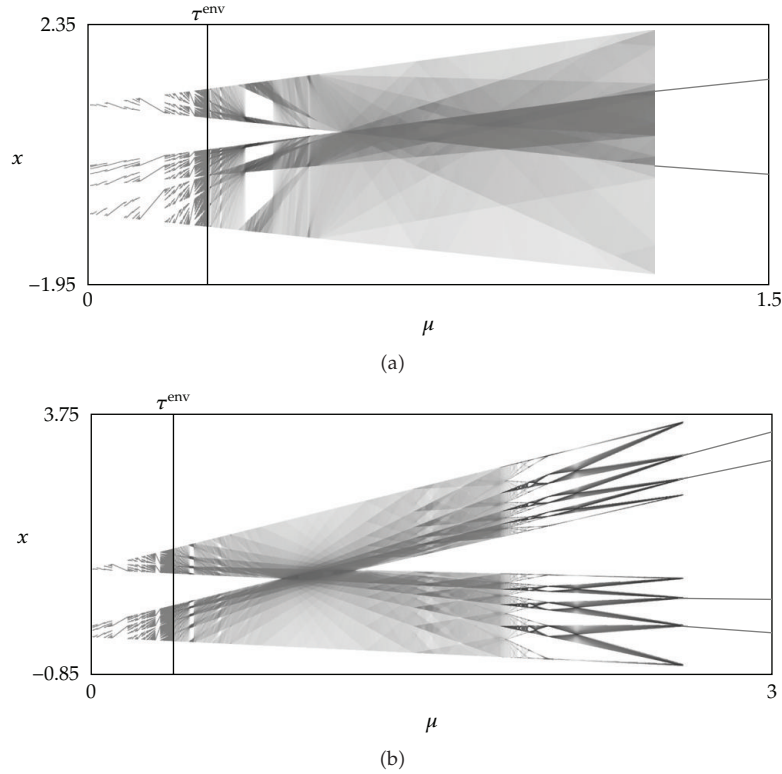
Figure 3: Numerically calculated bifurcation diagrams for $a = -0.42$, $b = -1.8$, $\mu = 0 \cdots 1.5$ (a) and $a = -0.42$, $b = -1.195$, $\mu = 0 \cdots 3.0$ (b). Both show similar structures in the left part, while they are significantly different in the right part. The location of these scans in the (b, μ)-plane is shown in Figure 2(c) with dashed lines. The line A corresponds to (a) and the line C to (b).

the two periodic scenarios in system (1.3), we do not investigate this part of the parameter space and restrict our investigation to region (3.2).

Figure 2 shows the bifurcation structure of the region P in three characteristic cases $a < 0$, $a = 0$ and $a > 0$. As one can see, in the case $a = 0$ the complete (b, μ)-plane is covered by the periodic domain, which is in this case formed by $\mathcal{M}^{2D}(B_1)$ and $\mathcal{M}^{2D}(B_2)$. By contrast, in both cases $a < 0$ and $a > 0$ there is a chaotic domain Q^{ch} (characterized by a positive Lyapunov exponent) located between the influence regions of B_1 and B_2. As one can see in Figure 3, the chaotic domain Q^{ch} has a complex interior structure formed by both one-band and multiband chaotic attractors. However, in [24] this structure is not investigated. Therefore the question arises, which bifurcation phenomena form the interior structure of the chaotic domain.

It is worth noticing that the above-mentioned question in the case of the negative jump of the system function ($l = -1$) is already investigated. The behavior close to the boundary between the period adding structure and the chaotic domain is reported in [23]. The map considered in this work is equivalent to a special case of map (1.1) with identical slopes a and b. However, the obtained results are also valid for any values of a and b. It is shown in the cited work that the chaotic domain is organized in this case by the bandcount-adding scenario, which is formed by interior crises [31]. A part of these crises is caused

by the unstable periodic orbits originating from the periodic domain where they are stable and organized by the period adding scenario. Additionally, the interior substructures of the bandcount-adding scenario are formed by interior crises caused by periodic orbits, which are everywhere unstable. Since map (1.3) shows also a transition from period adding to chaos, it can be expected, that the chaotic domain is in this case also organized by the bandcount-adding scenario.

The behavior close to the transition from the periodic domain organized by the period increment scenario with coexisting attractors to chaos for map (1.1) in the case $l = -1$ is investigated in a series of works [20–22]. It is shown that the structure of the chaotic domain is organized in this case by two types of crises, namely band-merging crises and interior crises. The unstable periodic orbits originating from the periodic domain lead to band-merging crises organized by the bandcount-increment scenario, whereas the everywhere unstable orbits lead to interior crises forming the interior substructures of this scenario. The bandcount-increment scenario is significantly more complex than the bandcount-adding scenario and is closely related to the composite and nonsmooth shape of the boundary between periodic and chaotic domain. In contrast to the case of the bandcount-adding scenario where this boundary represents a smooth surface, in the case of the bandcount-increment scenario the boundary is given by segments of bifurcation surfaces of two types (border-collision bifurcations and degenerated flip bifurcations). Therefore, the question arises, up to which extent the results obtained for the case $l = -1$ can be adopted also for the case $l = +1$ considered in the present work.

4. Periodic Domain

As the bifurcation structure of the chaotic domain is influenced by the periodic orbits, which exist in the adjacent periodic domain, let us recall some results related to the bifurcation structure of this periodic domain. For a more detailed description we refer to [24].

As mentioned above, the periodic domain of system (1.3) in the region P of the parameter space is organized by two codimension-3 big bang bifurcation points, B_1 and B_2 (see Figure 2). In the case $a = 0$ the influence region of each of these points consists of a two-dimensional manifold, which together cover the complete (b, μ)-plane and are both organized by the pure period increment scenario. The boundary between the manifolds $\mathcal{M}^{2D}(B_1)$ and $\mathcal{M}^{2D}(B_2)$ is given by the curve

$$\tau^\infty = \left\{ (a, b, \mu) \mid a = 0, \ b < -1, \ \mu = -\frac{1}{b} \right\}, \tag{4.1}$$

which is shown in Figure 2(b).

Below τ^∞ the influence region of the big bang point B_1 is located. It consists of an infinite number of stability regions of periodic orbits with odd periods, beginning with $P^s_{\mathcal{L}\mathcal{R}^2}$ and continuing with $P^s_{\mathcal{L}\mathcal{R}^{2n}}$ for $n > 1$. Above τ^∞, the influence region of the big bang bifurcation point B_2 is located. It is structured similarly to the influence region of B_1, consisting of an infinite number of stability regions of periodic orbits with even periods, beginning with $P^s_{\mathcal{L}\mathcal{R}}$ and continuing with $P^s_{\mathcal{L}\mathcal{R}^{2n+1}}$ for $n > 1$.

In the case $a \neq 0$, $\Omega(B_1)$ as well as $\Omega(B_2)$ are no longer structured by the pure period increment scenario. Note that, however, both regions still contain the stability regions of the same orbits as before. In the case $a > 0$, $\Omega(B_2)$ is structured by the period increment scenario

with coexisting attractors. Since system (1.3) is piecewise linear and has only one point of discontinuity, at most two attractors may coexist. In this case, this means that the regions $P^s_{\mathcal{LR}^{2n+1}}$ overlap pairwise. The region $\Omega(B_1)$ is structured by the period adding scenario, that means between two subsequent regions $P^s_{\mathcal{LR}^{2n}}$ and $P^s_{\mathcal{LR}^{2n+2}}$ there is some free space where the stability regions of the orbits are located, which can be generated by the infinite symbolic sequence adding scheme. Note that the infinite symbolic sequence adding scheme can be considered as a symbolic representation of the well-known Farey-tree [39, 42, 43], which is a subtree of the Stern-Brocot-tree [44, 45]. In the case $a < 0$ the situation is reversed, with $\Omega(B_2)$ structured by the period adding scenario and $\Omega(B_1)$ structured by the period increment scenario with coexisting attractors. In both cases, the chaotic domain appears between the two influence regions, centered at the former location of the curve τ^∞. For $|a| \to 1$, both influence regions $\Omega(B_1)$ and $\Omega(B_2)$ shrink and their boundaries move away from each other in the direction of the respective big bang bifurcation points. Since the bifurcation scenarios in both cases $a > 0$ and $a < 0$ are identical, we consider in the following only the case $a > 0$.

For the analytical calculations in the following we will need some periodic orbits of system (1.3). It can be easily seen that system (1.3) has at most two fixed points, however only the fixed point

$$x^{\mathcal{R}} = \frac{\mu + 1}{1 - b} \tag{4.2}$$

exists in the parameter space region P. Since we consider $b < -1$, the fixed point $x^{\mathcal{R}}$ is unstable.

The existence regions of the $(n + 1)$-periodic orbits $O_{\mathcal{LR}^n}$ are bounded by the surfaces of border collision bifurcations where the involved orbit collides with the boundary $x = 0$ from the left with its first point $x_0^{\mathcal{LR}^n}$ and from the right with its next to last point $x_{n-1}^{\mathcal{LR}^n}$. In the following these surfaces will be denoted by $\xi^{0,\ell}_{\mathcal{LR}^n}$ and $\xi^{n-1,r}_{\mathcal{LR}^n}$, respectively. As system (1.3) is piecewise linear, the orbits $O_{\mathcal{LR}^n}$ and hence the border collision bifurcation surfaces can be calculated analytically for all $n > 0$. The colliding points $x_0^{\mathcal{LR}^n}$ and $x_{n-1}^{\mathcal{LR}^n}$ are:

$$x_0^{\mathcal{LR}^n} = -\frac{(b^{n+1} - 1)\mu + (b^n - 1)}{(ab^n - 1)(b - 1)},$$

$$x_{n-1}^{\mathcal{LR}^n} = ab^{n-2}x_0 + \frac{(b^{n-1} - 1)\mu + (b^{n-2} - 1)}{b - 1}. \tag{4.3}$$

(see [24]) The conditions $x_0^{\mathcal{LR}^n} = 0$ and $x_{n-1}^{\mathcal{LR}^n} = 0$ lead us to the following expressions for the border collision bifurcation surfaces $\xi^{0,\ell}_{\mathcal{LR}^n}$ and $\xi^{n-1,r}_{\mathcal{LR}^n}$. These expressions are valid regardless to which influence region $\Omega(B_{1,2})$ the corresponding border collision bifurcation surfaces belong and in which bifurcation scenarios these surfaces are involved in

$$\xi^{0,\ell}_{\mathcal{LR}^n} = \left\{ (a, b, \mu) \mid |a| < 1, \ b < -1, \ \mu = -\frac{b^n - 1}{b^{n+1} - 1} \right\}, \tag{4.4}$$

$$\xi^{n-1,r}_{\mathcal{LR}^n} = \left\{ (a, b, \mu) \mid |a| < 1, \ b < -1, \ \mu = -\frac{b^{n-2}(1 - a) - 1 + ab^n}{b^{n-2}(b - a) - 1 + ab^n} \right\}. \tag{4.5}$$

The orbits $O_{\mathcal{LR}^n}$ are not everywhere stable in their existence regions $P_{\mathcal{LR}^n}$. The boundary between the region in which an orbit $O_{\mathcal{LR}^n}$ is stable and the region in which it is unstable is given by one of the bifurcation subspaces

$$\theta^{\pm}_{\mathcal{LR}^n} = \left\{ (a, b, \mu) \mid ab^n = \pm 1 \right\}. \tag{4.6}$$

Note that an orbit $O_{\mathcal{LR}^n}$ involved in the period increment scenario with coexisting attractors (that means with odd n for $a > 0$ and even n for $a < 0$) becomes unstable via degenerated flip bifurcation [46] at the boundary $\theta^{-}_{\mathcal{LR}^n}$. By contrast, an orbit $O_{\mathcal{LR}^n}$ involved in the period adding scenario (with odd n for $a < 0$ and even n for $a > 0$) becomes unstable at the boundary $\theta^{+}_{\mathcal{LR}^n}$. Note that $\theta^{+}_{\mathcal{LR}^n}$ represents a codimension-2 bifurcation given by the intersection curve of the bifurcation surfaces $\xi^{0,\ell}_{\mathcal{LR}^n}$ and $\xi^{n-1,r}_{\mathcal{LR}^n}$ located at the surface τ^{env} (for details see [47]).

When dealing with the period increment scenario with coexisting attractors, it is necessary to know, which boundaries of its regions correspond to which border collision bifurcations. In the case $a > 0$ the upper boundary of the region $P_{\mathcal{LR}^{2n+1}}$ is given by the surface $\xi^{n-1,r}_{\mathcal{LR}^n}$ and the lower boundary by the surface $\xi^{0,\ell}_{\mathcal{LR}^n}$.

As one can see in Figure 2(c) the surfaces detected so far form the boundary between $\Omega^{\text{inc}}(B_2)$ and the chaotic domain. In the case $a > 0$ this boundary consists of pieces of the border collision bifurcation surfaces $\xi^{0,\ell}_{\mathcal{LR}^n}$ and pieces of the stability boundaries $\theta^{-}_{\mathcal{LR}^{2n+1}}$. The boundary between the region $\Omega^{\text{add}}(B_1)$ and the chaotic domain is given by the smooth surface

$$\tau^{\text{env}} = \left\{ (a, b, \mu) \mid |a| < 1, \ b < -1, \ \mu = \frac{1-a}{a-b} \right\}, \tag{4.7}$$

which follows from the condition $f_\ell(f_r(0)) = f_r(f_\ell(0))$. Note that $\tau^{\text{env}} \equiv \tau^{\infty}$ for $a = 0$.

5. General Properties of the Chaotic Domain

Continuing the work reported in [24], we investigate the structure of (b, μ) parameter subspace of system (1.3) for specific values of a. Typical examples for the bifurcation scenarios calculated numerically by varying μ are shown in Figure 3. The presented examples correspond to the lines marked with A and C in Figure 2(c). Note that the bifurcation scenarios, which can be obtained for other values of a and b are in the most cases similar to the presented examples.

As one can see, both diagrams have parts that are similar to each other, and parts which differ. In the left part of both diagrams we observe the period adding structure already mentioned in Section 4. For increasing values of μ there is a region which apparently contains a two-band chaotic attractor, that is interspersed with chaotic attractors with higher bandcounts. Increasing μ further, we observe a crisis bifurcation where the bands of the two-band attractor merge and an one-band attractor emerges. Afterwards the two diagrams begin to differ. In Figure 3(a), the one-band attractor persists until the dynamic becomes periodic again at the boundary between chaotic domain and the region organized by the period increment scenario with coexisting attractors as mentioned in Section 4. In Figure 3(b), however, one more crisis bifurcation leads to the appearance of another two-band chaotic attractor. Like the two-band attractor next to the period adding scenario, this attractor is interrupted by chaotic attractors with higher bandcounts. The crises, which induce these

(a) $a > 0$

(b) $a < 0$
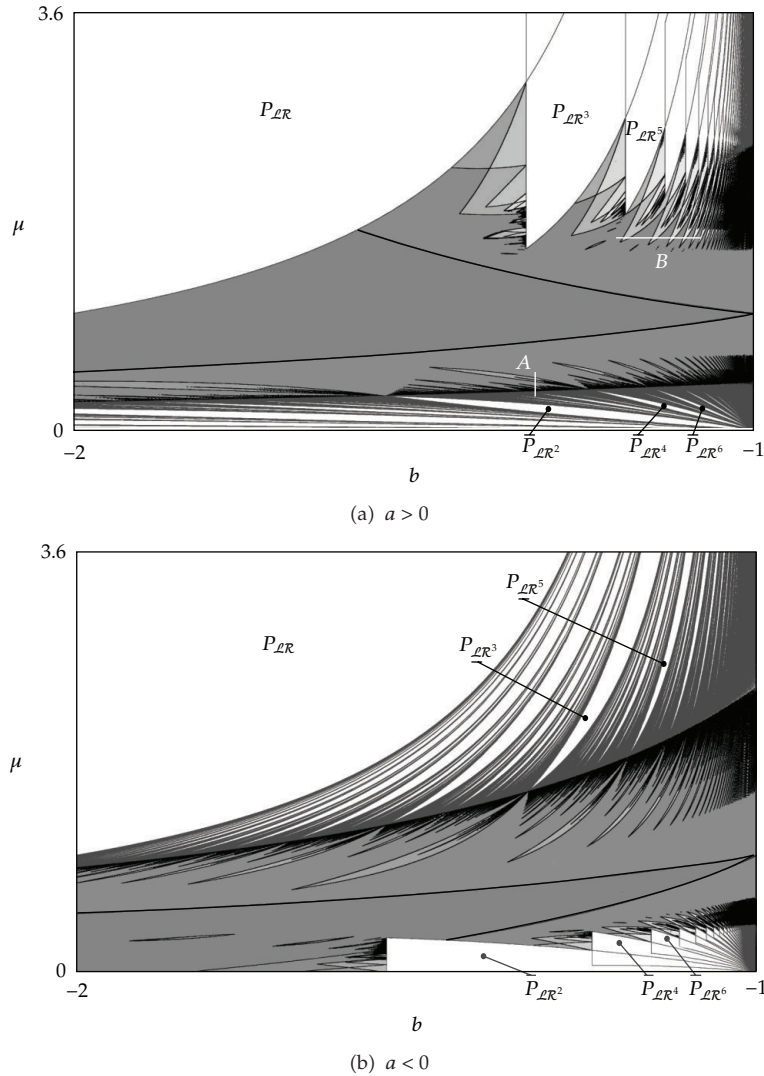
Figure 4: Numerically calculated bandcount diagrams in the 2D parameter space for $a = 0.42$ (a), $a = -0.42$ (b) and $b = -2.0 \cdots -1.0$, $\mu = 0 \cdots 3.6$, showing the basic bifurcation structure of the chaotic domain. The periodic domain is colored white, the chaotic domain in various shades of gray. The gray tones represent the bandcount of the regions, calculated using the numeric approach reported in [48]. The lighter the gray of a chaotic region the higher its bandcount is. The white lines in (a) show the locations of two bifurcation scenarios, shown in Figures 9 and 14.

high-bandcount attractors look different than the crises, which induce the high-bandcount attractors in the left part of the figure. Also, the whole structure is more complex.

Based on these observations, we divide the chaotic domain into three subregions. We call the region adjacent to the period adding scenario Q^{add}, the single-band region Q^1 and the region next to the period increment scenario Q^{inc}.

It seems to be a hard if not an unsolvable task to explain the presented bifurcation scenarios based on the one-dimensional bifurcation diagrams only. Since a one-dimensional

bifurcation diagram is limited in the amount of information it can reveal about two-dimensional structures in the parameter space, we determined bandcounts numerically using the algorithm reported in [48] in relevant parts of a (b, μ)-plane (see Figure 4). Note that this figure shows the same region in the parameter space as Figure 2. In this figure, the three regions we have identified above are clearly visible, as are the structures within and the boundaries between them. Furthermore it becomes clearly visible that the chaotic domain shown as a homogeneous gray region in Figure 2 has a well-organized interior structure.

5.1. Region Boundaries

The outer boundaries of Q^{ch} are already given through the boundaries of the periodic domain. One of these boundaries is defined through the surface τ^{env}. The other boundary is defined through the union of parts of the lower boundaries of the regions $P^s_{\mathcal{LR}^{2n+1}}$ and parts of the stability boundaries $\theta^-_{\mathcal{LR}^{2n+1}}$ (see Section 4).

Our task is now to find the boundaries separating the region Q^1 from Q^{add} and Q^{inc}. As one can see in Figure 3, the bifurcation which defines these boundaries represents a band-merging crisis. Given the number of gaps in the attractor before the bifurcation—one—the unstable periodic orbit involved in this crisis is the unstable fixed point $x^{\mathcal{R}}$, (see (4.2)), as shown in Figure 5.

To calculate the crisis surfaces, the points of the appropriate kneading orbits are needed. For the band-merging crisis at the smaller value of μ, these are $x^{ko}_{\ell} = \mu$ and $x^{ko}_{\ell r} = b\mu + \mu + 1$. This band-merging crisis can thus be calculated by any of the conditions $x^{\mathcal{R}} = x^{ko}_{\ell}$ and $x^{\mathcal{R}} = x^{ko}_{\ell r}$. This leads to the boundary surface

$$\gamma_{\text{add}} = \left\{ (a, b, \mu) \mid 0 < |a| < 1, \ b < -1, \ \mu = -\frac{1}{b} \right\} \tag{5.1}$$

which separates the region Q^1 from the region Q^{add}.

It is worth noticing that for the calculation of the other band-merging crisis surface caused by the unstable fixed point $x^{\mathcal{R}}$ we have to use points of the other kneading orbit. As one can see in Figure 5, the kneading orbit points relevant for this crisis bifurcation are $x^{ko}_{r^2\ell} = a(b(\mu + 1) + \mu + 1) + \mu$ and $x^{ko}_{r^2\ell r} = b(a(b(\mu + 1) + \mu + 1) + \mu) + \mu + 1$. Hence, the band-merging crisis at the higher value of μ can be calculated by any of the conditions $x^{\mathcal{R}} = x^{ko}_{r^2\ell}$ and $x^{\mathcal{R}} = x^{ko}_{r^2\ell r}$. This leads to the boundary surface

$$\gamma_{\text{inc}} = \left\{ (a, b, \mu) \mid 0 < |a| < 1, \ b < -1, \ \mu = -\frac{a - ab^2 - 1}{a - ab^2 - b} \right\} \tag{5.2}$$

which separates the region Q^1 from the region Q^{inc}. The location of the surfaces γ_{add} and γ_{inc} in the plane (b, μ) is shown in Figure 6.

5.2. Boundary Surface Properties

Let us consider some properties of the crisis surfaces γ_{add} and γ_{inc}. It is noticeable that the surface γ_{add} can be seen as some kind of continuation of the curve τ^∞ for the case $a \neq 0$. Both
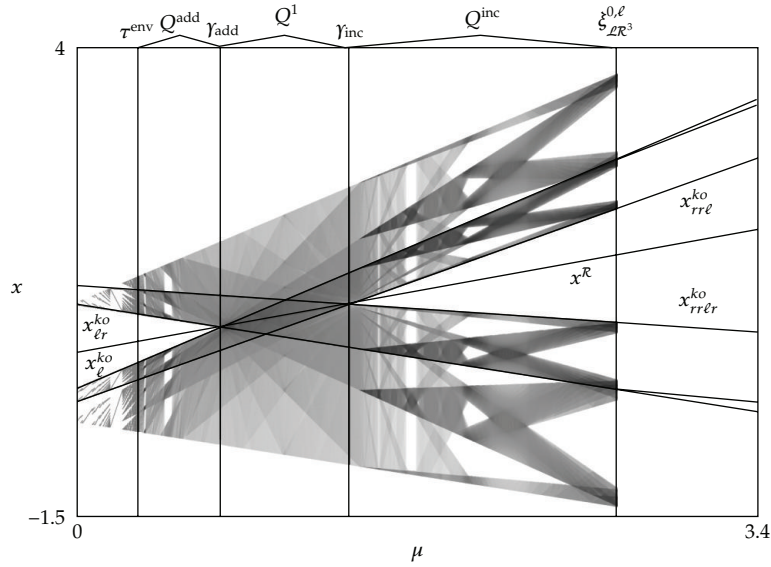
Figure 5: Numerically calculated bifurcation diagram for $a = 0.42$, $b = -1.37$, $\mu = 0 \cdots 3.4$, showing a typical part of the chaotic domain. The location of this scenario in the (b, μ)-plane is marked with B in Figure 2(c).
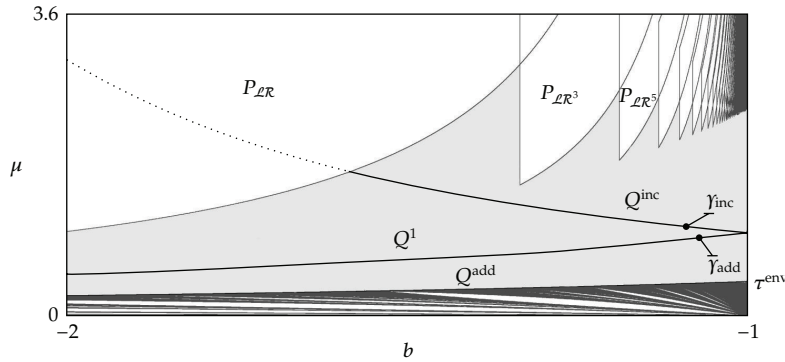
Figure 6: Numerically calculated structure of the (b, μ)-plane for $a = 0.42$, $b = -2.0 \cdots -1.0$, $\mu = 0 \cdots 3.6$. The two curves γ_{add} and γ_{inc} are analytically calculated and show the band-merging crisis curves structuring the chaotic domain. In the periodic domain, the curve γ_{inc} is shown dotted.

are defined through $\mu = -1/b$, and differ only in the value of a at which they exist. Since the value of μ in (5.1) does not depend on a, the location of the surface γ_{add} is the same in all (b, μ)-planes. Considering τ^{env}, this means that the area of the chaotic region between γ_{add} and τ^{env} tends to zero for $|a| \to 0$ and increases for $|a| \to 1$. Note that γ_{add} and τ^{env} never intersect, since they can only coincide at $a = 0$.

The behavior of γ_{inc} is more complicated. Like γ_{add}, it tends to τ^{env} for $|a| \to 0$ and is located far away from it for $|a| \to 1$. However, unlike γ_{add} its interaction with the boundary between the periodic and the chaotic domain is more sophisticated.

As described in Section 4, the periodic regions shrink for $|a| \to 1$. It is not readily apparent whether their boundary moves faster away from γ_{add} than γ_{inc}, so it is possible that γ_{inc} will intersect some periodic regions $P^s_{\mathcal{LR}^n}$ for some values of a. That it indeed does so can

be seen, for example, in Figure 6, which shows an intersection of γ_{inc} and the lower boundary of a periodic region ($P_{\mathcal{LR}}$, to be precise) for $a = 0.42$. So the question arises whether it is possible that γ_{inc} will intersect every periodic region $P_{\mathcal{LR}^{2n+1}}$ for appropriate values of a.

To confirm this, let us calculate the intersection of γ_{inc} with the lowest point of a stability region $P^s_{\mathcal{LR}^n}$. If this point can be found, γ_{inc} will intersect that region for smaller absolute values of a, and will not intersect it for larger values. To locate this point, we need the border collision bifurcation surfaces $\xi^{0,\ell}_{\mathcal{LR}^n}$ and the corresponding stability boundaries $\theta^-_{\mathcal{LR}^n}$.

In the case of $a > 0$, the lowest value of μ of a stability region $P^s_{\mathcal{LR}^{2n+1}}$ is at the intersection of its lower boundary with the stability boundary. We get that value of μ as a function of a and n by solving $\theta^-_{\mathcal{LR}^n}$ for b and inserting it into $\xi^{0,\ell}_{\mathcal{LR}^n}$. Since we want γ_{inc} to intersect $P^s_{\mathcal{LR}^{2n+1}}$ at the same point, we insert the same value b into γ_{inc} as well. This leads to:

$$\xi^{0,\ell}_{\mathcal{LR}^n}\Big|_{b=(-a^{-1})^{-1/n}} = \frac{1+a}{a\left((-a)^{-(n+1)/n} - 1\right)},$$

$$\gamma_{\text{inc}}\Big|_{b=(-a^{-1})^{-1/n}} = -\frac{-a + (-a)^{1-2/n} + 1}{-a + (-a)^{1-2/n} + (-a)^{-1/n}}. \tag{5.3}$$

Note that (5.3) is valid only for $a > 0$ in combination with odd values of n as well as for $a < 0$ in combination with even values of n. By solving $\xi^{0,\ell}_{\mathcal{LR}^n}\big|_{b=(-a^{-1})^{-1/n}} = \gamma_{\text{inc}}\big|_{b=(-a^{-1})^{-1/n}}$ for a, we get:

$$a^n_{\gamma_{\text{inc}}} = (-1)^{n+1}2^{-(1/2)n}, \tag{5.4}$$

which is the value of a at which γ_{inc} intersects the lowest point of the stability region $P^s_{\mathcal{LR}^n}$. The largest value $a^n_{\gamma_{\text{inc}}}$ can take is $a^1_{\gamma_{\text{inc}}} = 2^{-1/2} \approx 0.7071$. Because $|a^n_{\gamma_{\text{inc}}}|$ decreases monotonically for increasing n, approaching 0 for $n \to \infty$, we can conclude that γ_{inc} intersects every region $P^s_{\mathcal{LR}^n}$ for small enough absolute values of a. Consequently, a transition from the period-$(n+1)$ orbit $O_{\mathcal{LR}^n}$ to one-band chaos (as shown in the right part of Figure 3(a) for $n = 1$) is possible for any n.

Since γ_{inc} is the boundary between Q^1 and Q^{inc}, an intersection of γ_{inc} with a periodic region $P^s_{\mathcal{LR}^n}$ alters the general structure of Q^{ch}. Recall, that the intersection point of γ_{inc} with the boundary of the periodic domain $\Omega^{\text{inc}}(B_2)$ depends on the parameter b. For larger values of b than at the point of intersection, there is the region Q^{inc} between Q^1 and the period increment regions. For smaller values of b than at the point of intersection, the periodic domain overlaps with Q^1 so that there is no Q^{inc} for the values of b between an intersection with a periodic region $P^s_{\mathcal{LR}^n}$ and its stability boundary $\theta^-_{\mathcal{LR}^n}$. This is illustrated in Figure 7.

This explains the difference between the two bifurcation diagrams shown in Figure 3. Figure 3(a) corresponds to a value of b, which lies between the intersection of γ_{inc} with the boundary of a periodic region and the stability boundary belonging to that periodic region. At values of b, which are not between such a point of intersection and the corresponding stability boundary, all bifurcation diagrams of the chaotic domain calculated for constant values of a and b will look similar to Figure 3(b). They will contain at least a two-band attractor, which is adjacent to the region of period increment with coexisting attractors scenario.
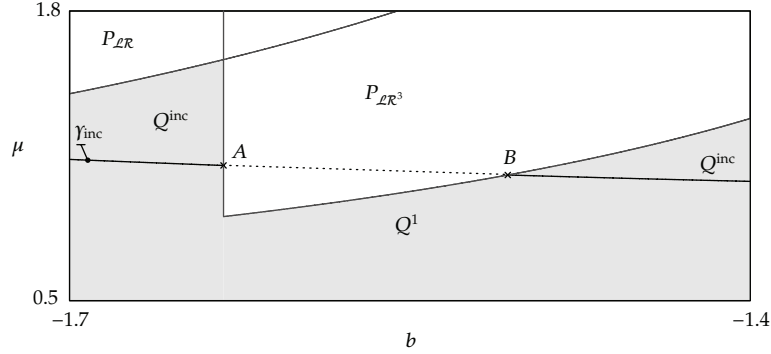
Figure 7: Analytically determined structure of the (b, μ)-plane for $a = 0.23$, $b = -1.7 \cdots -1.4$, $\mu = 0.5 \cdots 1.8$. The band-merging crisis curve γ_{inc} intersects the periodic region $P^s_{\mathcal{LR}^3}$. Between the two intersection points marked with A and B, Q^1 is adjacent to the periodic region. For values of b smaller than A or larger than B, Q^1 is adjacent to Q^{inc} instead.

6. Bandcount Adding Region

At this point the question may arise, why we distinguish between the two regions Q^{add} and Q^{inc}. The main reason for that is that the bifurcation structure of these regions emerges at the boundary to the corresponding adjacent periodic regions and depends strongly on the fact how these periodic regions are structured.

In this section we turn to the bifurcation structure of the region Q^{add}, that is, the bifurcation structure occurring at the boundary to the adjacent period adding scenario. We will demonstrate below, that the bifurcation structure of this region is organized by the so-called bandcount-adding scenario, initially reported in [23]. In general, the region Q^{add} is bounded by the surfaces γ_{add} and τ^{env} (this can be seen in Figure 6 and in Figure 8 below). The distance between these surfaces shrinks with decreasing absolute value of a, so that the complete region of the bandcount-adding scenario shrinks more and more. It turns out, however, that this is the only effect of the parameter a.

Note that the bifurcation structure of the chaotic domain near the boundary to a periodic region organized by the period adding scenario in a different piecewise linear map is investigated in detail in [23]. In the cited work the bandcount-adding scenario was described and it is remarkable, although somehow expected, that the bifurcation structure in Q^{add} is organized similarly.

6.1. Overall Bandcount Adding Structure

The bifurcation structure of the region Q^{add} is shown in Figure 8. As it was demonstrated in [23], the overall bandcount-adding scenario is composed of two recursive, self-similar structures, the actual bandcount-adding scenario and the bandcount doubling scenario nested within. Note that we will denote the regions that form these scenarios as "bandcount-adding regions" and "bandcount doubling regions", respectively. The structure of the overall bandcount-adding scenario is closely connected to the structure of the adjacent period adding scenario. This is due to the fact that the stable orbits forming the period adding scenario in the periodic domain are not destroyed at the boundary to the chaotic domain. Instead, at this
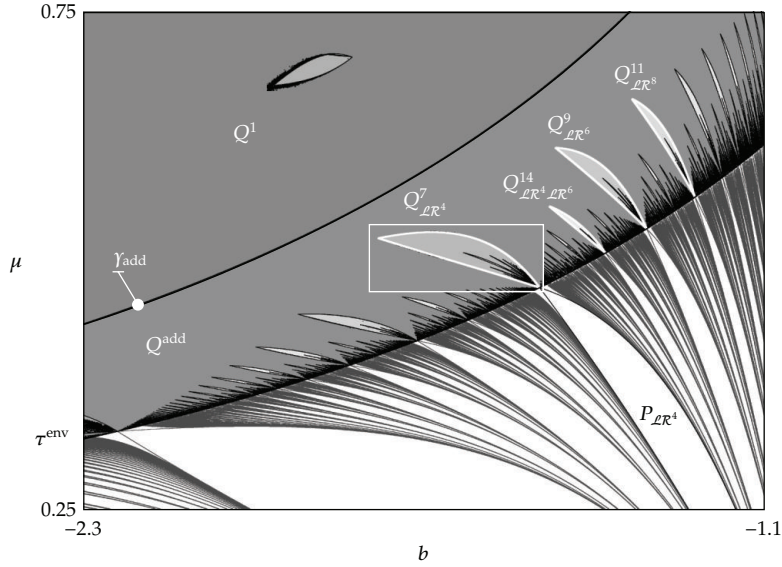
Figure 8: Numerically calculated bandcount diagram in the 2D parameter space for $a = 0.2$, $b = -2.3 \cdots -1.1$, $\mu = 0.25 \cdots 0.75$. Both the period adding (gray lines) and the bandcount-adding (gray areas) scenarios can be seen, separated by the boundary curve τ^{env}. The white curves inside the white box show the (analytically calculated) interior crisis curves $\eta^r_{\mathcal{LR}^4}$ and $\eta^\ell_{\mathcal{LR}^4}$, which are the boundaries of the bandcount-adding region $Q^7_{\mathcal{LR}^4}$. The other white curves show the interior crises corresponding to the respective labels. The band-merging crisis curve γ_{add} separates Q^{add} from Q^1. Note that the region in the upper part is an irregular region inside Q^1. The marked rectangle is shown enlarged in Figure 10.

boundary the orbits become unstable and are responsible for the crisis bifurcations forming the overall bandcount-adding scenario.

As an example in Figure 8 the region $P_{\mathcal{LR}^4}$ is shown, where the 5-periodic orbit $O_{\mathcal{LR}^4}$ is stable. The boundaries of this region are given by the border-collision bifurcation surfaces $\xi^{0,\ell}_{\mathcal{LR}^4}$ and $\xi^{3,r}_{\mathcal{LR}^4}$ of this orbit. As one can see, both curves intersect the boundary τ^{env} at the same point. Remarkably, at this point the region $Q^7_{\mathcal{LR}^4}$ originates, which is bounded by the crisis bifurcation surfaces caused by the same orbit $O_{\mathcal{LR}^4}$ but which is now unstable.

As one can clearly see in Figure 8, the described phenomenon occurs for each periodic orbit, which is stable within the periodic domain. Since these orbits are organized by the period adding scenario, the regions of multiband chaotic attractors are organized in a similar way. Recall, that the infinite symbolic sequence adding scheme which organizes this scenario, contains not only the first generation sequences, which are given in the considered case by $\mathcal{LR}^n$ with n even, but also of sequences of further generations, which result from the concatenation of their corresponding parent sequences. For example, the second generation sequences $\mathcal{LR}^n\mathcal{LR}^{n+2}$ result from the concatenation of their parent sequences $\mathcal{LR}^n$ and $\mathcal{LR}^{n+2}$. Consequently, the overall structure can be defined recursively and consists therefore of an infinite number of generations. This fact is reflected in the structure of the chaotic domain. This means that there is a first generation of regions that stretches over the complete bandcount-adding region Q^{add} (namely the regions of the orbits with the sequences $\mathcal{LR}^n$, n even) and there are regions of higher generations, which are located between the regions of the lower generations. For example, the second generation regions are located between

the first generation regions, the third generation regions are located between the second generation regions, and so on, ad infinitum. Figure 8 shows this.

The procedure for the analytical calculation of the regions forming the overall bandcount-adding scenario is described in detail in [23]. In this work it is shown that the boundaries of these regions are given by interior crisis bifurcations, which occur at parameter values where the corresponding unstable periodic orbits collide with the chaotic attractor. An example for this is shown in Figure 9, by the collision of the period-5 orbit $O_{\mathcal{LR}^4}$ with the 7-band chaotic attractor. Note that the figure shows also that the orbit becomes virtual (which means that one of its points leaves its domain of definition according to to the symbolic sequence of the orbit, and therefore the orbit disappears) at the parameter values where one of its points is located on the boundary of the chaotic attractor. The explanation for that lies in the definition of border collision bifurcations, namely that one point of the orbit hits the boundary $x = 0$. This means that another point is given by $f_d(0)$, with $d \in \{\ell, r\}$. However, this is also a point of a kneading orbit of the system given by (1.3), which has the property to jump between the boundaries of the chaotic attractor. Therefore, for system (1.3) at a border collision bifurcation, which happens within the chaotic domain, one point of the colliding orbit is always located at a boundary of the chaotic attractor.

Consequently, the boundaries of the region $Q^7_{\mathcal{LR}^4}$ can be determined using the condition that a point of the orbit $O_{\mathcal{LR}^4}$ hits the boundary of the chaotic attractor, which is given by an appropriate point of the kneading orbit. Since the investigated system is piecewise linear, similar calculations can be performed for all basic orbits $O_{\mathcal{LR}^n}$ analytically. In this way we obtain the boundaries of all regions $Q^{n+3}_{\mathcal{LR}^n}$, which form the first generation of the bandcount-adding scenario:

$$
\eta^r_{\mathcal{LR}^n} = \left\{ (a,b,\mu) \mid 0 < |a| < 1, \ b < -1, \ \mu = -\frac{(b^{n+2}-1)a - b^2 + 1}{(b^{n+3}-1)a - b^3 + b} \right\}, \tag{6.1}
$$

$$
\eta^\ell_{\mathcal{LR}^n} = \left\{ (a,b,\mu) \mid 0 < |a| < 1, \ b < -1, \right.
$$

$$
\left. \mu = -\frac{(b^{n+2}-b^n)a^2 + (b^n - 2b^2 + 1)a - 1 + b^2}{(b^{n+2}-b^n)a^2 + (b^{n+1} - 2b^2 + 1)a - b + b^3} \right\}. \tag{6.2}
$$

As Figure 8 shows, the number of bands in each region $Q^{n+3}_{\mathcal{LR}^n}$ is equal to $p + 2$ where p is the period of the periodic orbit $O_{\mathcal{LR}^n}$ causing the crisis bifurcations. This represents a difference to the scenario described in [23], since in this work this number is equal to $p + 1$. The difference is easily explained taking into account that the p-periodic orbit determines the number of gaps between the bands, and hence the number of bands is $p + 1$. In the case of system (1.3) considered here, there is one additional gap (see Figure 9) occupied by the unstable fixed point $x^{\mathcal{R}}$, everywhere in Q^{add}.

In summary, a first generation region $Q^{n+3}_{\mathcal{LR}^n}$ of the overall bandcount-adding scenario is induced by the orbit $O_{\mathcal{LR}^n}$ and hence bounded by the interior crisis surfaces $\eta^\ell_{\mathcal{LR}^n}$, $\eta^r_{\mathcal{LR}^n}$. It is located next to the stability region $P^s_{\mathcal{LR}^n}$ and has a bandcount of $n + 3$.

The regions of the higher generations have similar properties. They are also induced by unstable orbits that are stable in the adjacent periodic domain and they are also located
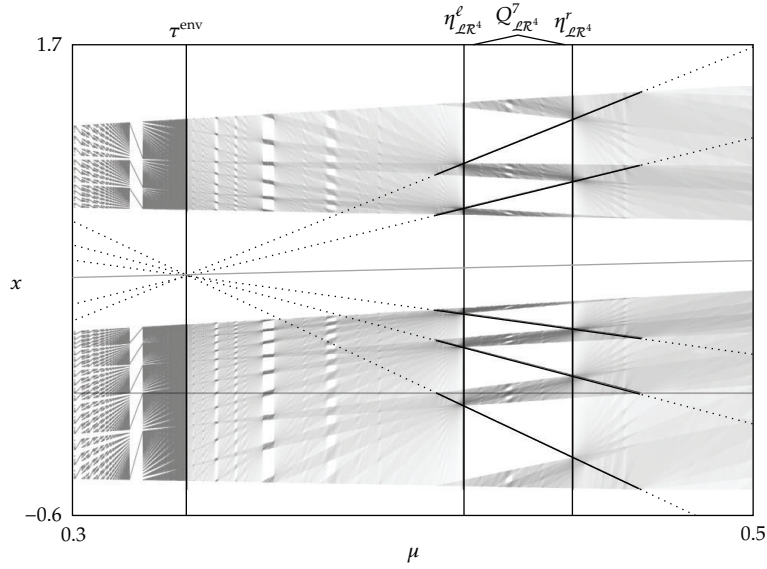
Figure 9: Numerically calculated bifurcation diagram for $a = 0.42$, $b = -1.32$, $\mu = 0.3 \cdots 0.5$. The curves show the unstable periodic orbit $O_{\mathcal{LR}^4}$ (black lines), which collides with the chaotic attractor in two interior crisis bifurcations, and the unstable fixed point $x^{\mathcal{R}}$ (gray line), which occupies the remaining gap. Note that the orbit is destroyed through border collisions at $x = 0$. Its nonexistent or virtual parts are shown dashed. The location of this scenario in the (b, μ)-plane is marked with A in Figure 4(a).

next to the stability region of these orbits. The symbolic sequences of these orbits can be determined using the infinite sequence adding scheme, as described in [24]. As an example, for each n, between the first generation regions $Q_{\mathcal{LR}^n}^{n+3}$ and $Q_{\mathcal{LR}^{n+2}}^{n+5}$ there is a region $Q_{\mathcal{LR}^n \mathcal{LR}^{n+2}}^{2n+6}$ of the second generation, and so on, ad infinitum. As an example for the regions of the second generation the region $Q_{\mathcal{LR}^4 \mathcal{LR}^6}^{14}$ is labeled in Figure 8.

6.2. Nested Substructures

Within each of the regions forming the overall bandcount-adding structure, there is a nested sequence of regions with higher bandcounts organized by the bandcount doubling scenario. The boundaries of the regions in this scenario are induced by interior crisis bifurcations as already pointed out in [23]. As an example, Figure 10 shows the bifurcation structures located within the region $Q_{\mathcal{LR}^4}^7$. The first two regions of the bandcount doubling scenario are the region $Q_{\mathcal{LR}^2 \mathcal{LR}^6}^{17}$ located in the middle part of $Q_{\mathcal{LR}^4}^7$ and the region $Q_{\mathcal{LR}^6 \mathcal{LR}^4 \mathcal{LR}^2 \mathcal{LR}^4}^{37}$ located in the middle part of $Q_{\mathcal{LR}^2 \mathcal{LR}^6}^{17}$.

The regions forming the bandcount doubling scenario originate at the same point (the intersection of the boundary surfaces with τ^{env}) as their surrounding regions and are located, roughly speaking, in the middle of them. Each region in the bandcount doubling scenario has the property that it is induced by an orbit with a period that is twice as high as the period of the orbit that induces the region surrounding it. Also, each of these regions contains the next region, following the same rules concerning bandcount and location, and so on, ad infinitum. Note that most of the regions in such a doubling-cascade are very hard to detect numerically because their size decreases rapidly.
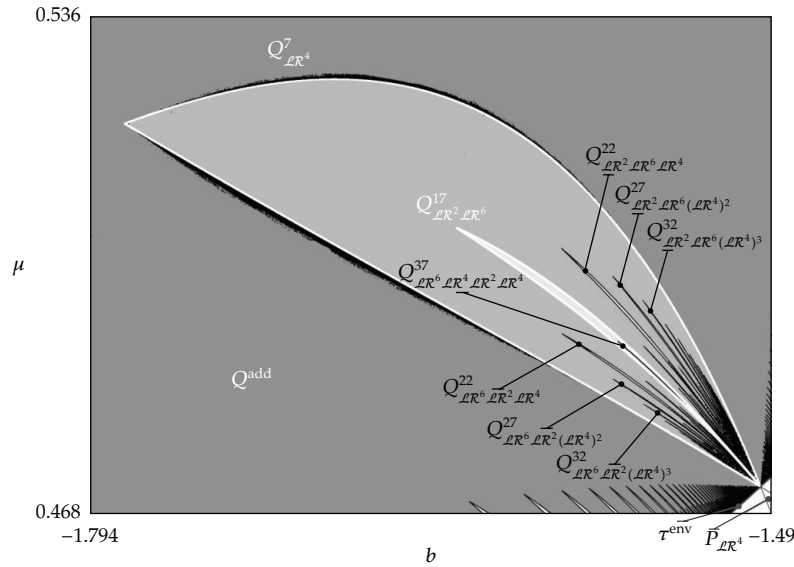
Figure 10: Numerically calculated bandcount diagram in the 2D parameter space for $a = 0.2$, $b = -1.794 \cdots -1.49$, $\mu = 0.468 \cdots 0.536$. The bandcount-adding region $Q^7_{\mathcal{L}\mathcal{R}^4}$ is shown enlarged. The bandcount doubling region $Q^{17}_{\mathcal{L}\mathcal{R}^2\mathcal{L}\mathcal{R}^6}$ is visible in the middle. The first three regions of both nested bandcount-adding structures to the left and to the right of $Q^{17}_{\mathcal{L}\mathcal{R}^2\mathcal{L}\mathcal{R}^6}$ are labeled. The second bandcount doubling region $Q^{37}_{\mathcal{L}\mathcal{R}^6\mathcal{L}\mathcal{R}^4\mathcal{L}\mathcal{R}^2\mathcal{L}\mathcal{R}^4}$ is also labeled. The rectangle in Figure 8 shows where this figure is located in the overall bandcount-adding scenario. The analytical Figure 11 corresponds to this image.

This shrinking of the regions is analogous to the behavior of the bandcount doubling investigated in [23]. In this work, the scaling constant for the length of the regions is analytically determined to be 2, whereas the scaling constant for the width of the regions does not exist, because its value tends to ∞ explaining the rapid shrinking of the size of the regions. Since the expressions of the crisis bifurcations involved in the bandcount doubling scenario in system (1.3) are significantly more complicated than it is the case for the system investigated in [23], it is very difficult to determine the scaling constants analytically. However, since the bandcount doubling regions in system (1.3) decrease in size in a similar way as the regions in the cited work (with the length of the regions decreasing by an approximately constant factor in each step in the sequence and the width of the regions decreasing stronger with each step), we can assume that the scaling constants are similar too. This means, that there exists a finite scaling constant corresponding to the length of the regions and there exists no finite scaling constant corresponding to the width of the regions. The bandcount doubling regions $Q^{17}_{\mathcal{L}\mathcal{R}^2\mathcal{L}\mathcal{R}^6}$ and $Q^{37}_{\mathcal{L}\mathcal{R}^6\mathcal{L}\mathcal{R}^4\mathcal{L}\mathcal{R}^2\mathcal{L}\mathcal{R}^4}$ shown in Figure 10 illustrate this.

The symbolic sequences of the orbits that induce the bandcount doubling regions can be determined using the creation rules presented in [23]. Note that the orbits corresponding to these sequences do not occur in the adjacent period adding scenario but emerge at the boundary τ^{env} between the periodic and the chaotic domain. Their regions of existence are bounded by two border-collision bifurcation surfaces and can be determined in the same way as it can be done for the orbits of the period adding scenario.

To give an example for the bandcount doubling scenario, we describe the first steps of the scenario inside the region $Q^7_{\mathcal{L}\mathcal{R}^4}$ shown in Figure 10. The first region inside $Q^7_{\mathcal{L}\mathcal{R}^4}$ has

a bandcount of 17 and is induced by the orbit $O_{\mathcal{LR}^2\mathcal{LR}^6}$. The number of bands in this region results from the fact, that 5 gaps of the attractor are occupied by the orbit $O_{\mathcal{LR}^4}$, 10 further gaps by the $O_{\mathcal{LR}^2\mathcal{LR}^6}$, and one gap by the fixed point $x^{\mathcal{R}}$.

Using the creation rules for the symbolic sequences mentioned above, it can be easily shown that the next two steps of the scenario are caused by the orbits $O_{\mathcal{LR}^6\mathcal{LR}^4\mathcal{LR}^2\mathcal{LR}^4}$ and $O_{\mathcal{LR}^6\mathcal{LR}^4\mathcal{LR}^2\mathcal{LR}^6\mathcal{LR}^2\mathcal{LR}^4\mathcal{LR}^6\mathcal{LR}^2}$ with periods 20 and 40, respectively. The bandcounts in the corresponding regions are 37 and 77, respectively, and can be explained by the number of gaps of the multiband attractors which are occupied by the unstable periodic orbits involved in the cascade up to a certain period including the unstable fixed point. Hence the bandcounts are given by $37 = (20 + 10 + 5 + 1) + 1$ and $77 = (40 + 20 + 10 + 5 + 1) + 1$, respectively.

This concludes the description of the bandcount doubling scenario. However, there are still nested substructures left to describe. As can be seen in Figure 10, there are several regions located within the region $Q^7_{\mathcal{LR}^4}$ on both sides of the bandcount doubling region $Q^{17}_{\mathcal{LR}^2\mathcal{LR}^6}$. These regions form a nested bandcount-adding scenario. The symbolic sequences of the orbits that induce these additional nested regions can be determined using the infinite sequence adding scheme. The starting sequences of this adding scheme correspond to the sequences of the bandcount doubling region and its surrounding region. Note that the sequences on one side of the region $Q^{17}_{\mathcal{LR}^2\mathcal{LR}^6}$ are slightly different from the sequences on the other side. In both cases, the sequence of the surrounding region $Q^7_{\mathcal{LR}^4}$ is concatenated several times, but the sequence of the bandcount doubling region $Q^{17}_{\mathcal{LR}^2\mathcal{LR}^6}$ in one case is shifted with respect to the other case. This can be seen in Figure 10: while the symbolic sequences to the left of the bandcount doubling region $Q^{17}_{\mathcal{LR}^2\mathcal{LR}^6}$ form the family $\mathcal{LR}^6\mathcal{LR}^2(\mathcal{LR}^4)^n$, the sequences to the right form the family $\mathcal{LR}^2\mathcal{LR}^6(\mathcal{LR}^4)^n$.

These families form the first generation of the nested bandcount-adding scenario. Further generations result from them in the same way as described for the overall bandcount-adding scenario. Note that these nested bandcount-adding regions have all the properties of the bandcount-adding regions described earlier. In particular, this means that each of these regions contains its own bandcount doubling cascade, and each of these bandcount doubling regions induce further nested bandcount-adding scenarios, which in turn contain bandcount doubling regions, and so on, ad infinitum. Additionally, each bandcount doubling region nested inside another region contains a nested bandcount-adding scenario, in a similar way as described above. This process continues ad infinitum, leading to a self-similar structure of the region Q^{add}.

7. Dynamics on the Boundary between the Period Adding Region and the Chaotic Domain

Using the analytical formulations of the interior crisis surfaces confining the overall bandcount-adding regions $Q^{|\sigma|+2}_\sigma$, we can observe that for each σ their right intersection point denoted in the following by ζ_σ belongs to the boundary surface τ^{env}. Recall that σ refers here to any basic sequence $\mathcal{LR}^n$ with n odd for $a > 0$, respectively even for $a < 0$, as well as to any sequence which can be derived from a pair $\mathcal{LR}^n$, $\mathcal{LR}^{n+2}$ using the sequence adding scheme. It can also be verified analytically that the surfaces of border collision bifurcation of the orbit O_σ which causes these crises, intersect the boundary surface τ^{env} at the same point. This is illustrated by Figure 8 which shows the boundaries of the bandcount-adding region $Q^7_{\mathcal{LR}^4}$ and the period adding region $P_{\mathcal{LR}^4}$. Since the orbit O_σ is stable within the periodic domain and unstable in the chaotic one, the stability boundary θ_σ intersects τ^{env} at the same point as

well. This means for example that

$$\zeta_{\mathscr{L}\mathscr{R}^n} = \eta^r_{\mathscr{L}\mathscr{R}^n} \cap \eta^\ell_{\mathscr{L}\mathscr{R}^n} \cap \tau^{\mathrm{env}} = \xi^{0,\ell}_{\mathscr{L}\mathscr{R}^n} \cap \xi^{n-1,r}_{\mathscr{L}\mathscr{R}^n} \cap \tau^{\mathrm{env}} = \theta_{\mathscr{L}\mathscr{R}^n} \cap \tau^{\mathrm{env}}. \tag{7.1}$$

Already this leads us to conclude that the points ζ_σ represent bifurcations with a codimension larger than one.

Next let us consider a point ζ_σ as a function of the third parameter a. Recall that the variation of a in the intervals $(-1,0)$ and $(0,1)$ does not change the topological structure of the regions $\Omega^{\mathrm{add}}(B_1)$ and Q^{add}. Hence, in the $3D$ parameter space (a,b,μ) each point at the curves $\zeta_\sigma(a)$ with $a \in (-1,0)$ and $a \in (0,1)$ represents a codimension-2 bifurcation Furthermore, it turns out that for any $a \in (-1,0)$ and $a \in (0,1)$ the points $\zeta_\sigma(a)$ represent codimension-2 big bang bifurcations. Recall that the region $Q^{|\sigma|+2}_\sigma$ contains an infinite number of nested subregions with higher bandcounts (bandcount doubling and nested bandcount-adding regions). All interior crisis surfaces bounding these regions originate from the point $\zeta_\sigma(a)$. In fact, not only the interior crisis surfaces but also the border collision bifurcation surfaces of the orbits responsible for these crises originate from the point $\zeta_\sigma(a)$. As a consequence, from each point $\zeta_\sigma(a)$ at the boundary τ^{env} originates an infinite number of existence regions of everywhere unstable periodic orbits.

As an example, Figure 11 shows a few of the curves forming the bifurcation structure emerging at the point $\zeta_{\mathscr{L}\mathscr{R}^4}$ (compare the the corresponding numeric results shown in Figure 10). The figure demonstrates the analytically calculated interior crises curves bounding the region $Q^7_{\mathscr{L}\mathscr{R}^4}$ and its nested substructures, namely the first two bandcount doubling regions $Q^{17}_{\mathscr{L}\mathscr{R}^2\mathscr{L}\mathscr{R}^6}$, $Q^{37}_{\mathscr{L}\mathscr{R}^6\mathscr{L}\mathscr{R}^4\mathscr{L}\mathscr{R}^2\mathscr{L}\mathscr{R}^4}$, as well as the first nested bandcount-adding regions $Q^{5n+17}_{\mathscr{L}\mathscr{R}^2\mathscr{L}\mathscr{R}^6(\mathscr{L}\mathscr{R}^4)^n}$ and $Q^{5n+17}_{\mathscr{L}\mathscr{R}^6\mathscr{L}\mathscr{R}^2(\mathscr{L}\mathscr{R}^4)^n}$ for $n = 1,2,3$. Additionally to these interior crises curves the existence boundaries or the corresponding unstable periodic orbits are shown as dashed curves. For sake of clarity only the border collision bifurcations involving the orbits responsible for crises bounding the doubling regions are labeled. The remaining 12 dashed curves define the border collision bifurcations involving the orbits responsible for crises bounding the nested bandcount-adding regions. Note that only the curves $\xi^{0,\ell}_{\mathscr{L}\mathscr{R}^4}$ and $\xi^{3,r}_{\mathscr{L}\mathscr{R}^4}$ exist on the right side of the stability boundary $\theta^+_{\mathscr{L}\mathscr{R}^4}$ where they confine the period adding region $P_{\mathscr{L}\mathscr{R}^n}$. All other border collision bifurcation curves originate from the point $\zeta_{\mathscr{L}\mathscr{R}^4}$ exist only on the left side of $\theta^+_{\mathscr{L}\mathscr{R}^4}$.

The question arises, how the system (1.3) behaves at the codimension-2 big bang bifurcations point ζ_σ. Calculating analytically the points of the orbit O_σ one obtains that at the point ζ_σ the expressions for these points become $0/0$ and hence indeterminate. As a consequence of this, there exists an absorbing set with positive Lebesgue measure, where each point belongs to an orbit O_σ. Since the point ζ_σ belongs to the stability boundary θ^+_σ, each of these infinite number of coexisting orbits O_σ is neutral (neither stable nor unstable). Among these orbits there are two special cases, namely the orbits undergoing the border collision bifurcations, which confine the region P_σ. These two orbits represent both kneading orbits which are in this case cyclic and represent the boundaries of the the absorbing set, so that the points of the other orbits which coexist with them are located between them.

This is illustrated by Figure 12 where the system function and its fifth iterated are shown at the point $\zeta_{\mathscr{L}\mathscr{R}^4}$ which is given for $a = 0.2$ by $b = -\sqrt[4]{1/a} \approx -1.49534878$, $\mu = (1-a)/(a-b) \approx 0.47187930$ (see (4.6) and (4.7)). In both Figures 12(a) and 12(b) the absorbing set is marked on the horizontal axis. As one can see, this set consists of two intervals which are bounded by the points of both kneading orbits starting with $f_\ell(0)$ and $f_r(0)$, as shown in
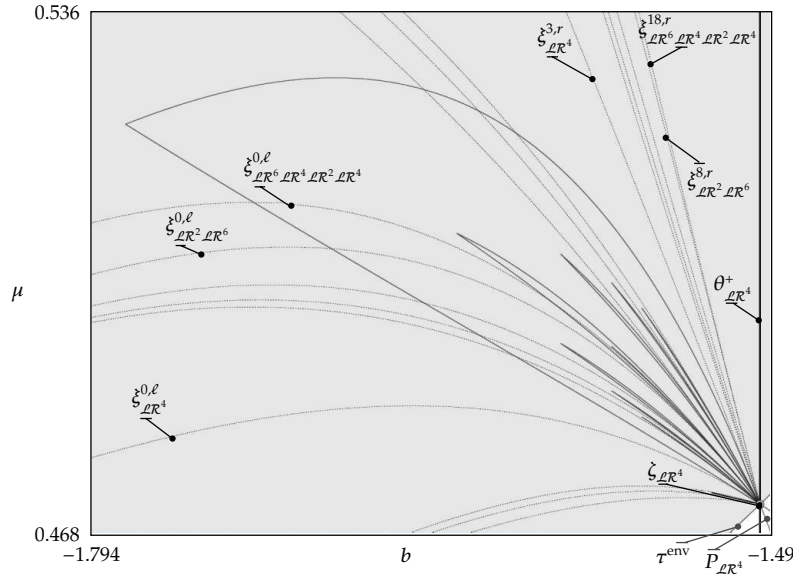
Figure 11: Analytically calculated bifurcation structure close to the big bang bifurcation point $\zeta_{\underline{\mathcal{L}\mathcal{R}}^4}$. Solid curves (except the boundary curve τ^{env} and the stability boundary $\theta^+_{\underline{\mathcal{L}\mathcal{R}}^4}$) refer to the interior crisis bifurcation curves, dashed curves—to the border collision bifurcation curved. For more details see text. The numerical Figure 10 corresponds to this image.
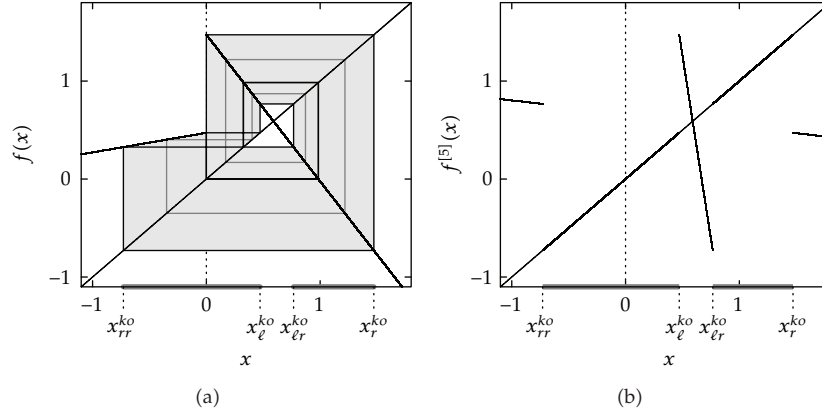
Figure 12(a). The behavior on the absorbing set becomes immediately clear by considering the fifth iterated function. As one can see in Figure 12(b), on this set the fifth iterated function coincide with the angle's bisector. Hence, each point on the absorbing set is a neutral fixed point for the fifth iterated and belongs to a neutral period-5 orbit of the original map. All these period-5 orbits correspond to the same symbolic sequence $\mathcal{L}\mathcal{R}^4$ as indicated in Figure 12(a).

Note finally that there is only a countable number of regions P_σ involved in the period adding scenario, and hence only a countable number of curves ζ_σ on the boundary surface τ_{env}. In the remaining noncountable set the behavior is aperiodic, corresponding to the limiting case ("infinite period") of the period adding structure.

8. Bandcount Increment Region

In this section we now turn to the bifurcation structure of the region Q^{inc}, that is, the bifurcation structure occurring at the boundary to the adjacent period increment scenario. As in the case of the bandcount-adding scenario, the parameter region Q^{inc} containing the so-called bandcount-increment scenario is bounded by the surfaces γ_{inc} and the envelope confining the period increment region, which is now a composite surface and more complicated than the envelope τ_{env} confining the period adding region. The distance between these surfaces shrinks with decreasing absolute value of a, so that also the complete region of the bandcount-increment scenario shrinks more and more. As in the case of the bandcount-adding scenario, this is the only effect of the parameter a.

The bandcount-increment scenario is much more complex than the bandcount-adding scenario and is investigated in detail in [20–22] for a different piecewise linear map, namely

Figure 12: Behavior at the big bang bifurcation point $\zeta_{\mathcal{LR}^4}$: system function (a) and its fifth iterated (b). On the horizontal axis the absorbing set containing an infinite number of coexisting neutral orbits $O_{\mathcal{LR}^4}$ is marked. In (a) three orbits are shown: two kneading orbits (in other words, the orbits $O_{\mathcal{LR}^4}$ undergoing border collision bifurcation) and one orbit located between them, which does not undergo a border collision bifurcation.

for the map (1.1) in the case $l = -1$. The bandcount-increment scenario in the cited works and the scenario investigated in this work share some properties, namely the triangular form of the regions, the overlap of adjacent regions, and some of the structures occurring inside the triangular regions.

The bandcount-increment scenario consists of triangular regions existing mainly between two consecutive periodic regions $P^s_{\mathcal{LR}^{n-2}}$ and $P^s_{\mathcal{LR}^n}$. In Figure 13(a) some triangular regions are labeled with their bandcounts 8, 10, and 12, using black numbers. There are also some additional, smaller regions, which are disconnected from the bigger triangles and which have also triangular shape. They are located directly below periodic regions and above the larger triangles. In Figure 13(a) some of these regions are labeled with their bandcounts 6, 8 and 10, using white numbers.

To explore the scenario, we start by counting the bandcounts in a sequence of large triangular regions (the results calculated numerically for b varied along the line marked with B in Figure 4(a) are shown in Figure 14, together with an appropriate bifurcation diagram). As can be seen, the bandcount of each region equals that of the preceding region increased by 2. The reason for that lies in the orbits that induce the crisis surfaces bounding the regions. As Figure 14 shows, these orbits are $O^u_{\mathcal{LR}^n}$ and collide with the attractor in band-merging crises (not in interior crises, as it was the case for the bandcount-adding scenario).

Note that a region, which is induced by such an orbit $O^u_{\mathcal{LR}^n}$ is not located adjacent to the periodic region $P_{\mathcal{LR}^n}$. Instead, it is located next to the periodic region $P_{\mathcal{LR}^{n-2}}$ one step to the left. This is illustrated in Figure 13(b), with $Q^8_{\mathcal{LR}^5}$ being located next to $P_{\mathcal{LR}^3}$, $Q^{10}_{\mathcal{LR}^7}$ next to $P_{\mathcal{LR}^5}$, and so on.

The procedure to determine these crises analytically is similar to the determination of the interior crises of the bandcount-adding scenario. We need to find appropriate kneading orbits that form the boundary of the chaotic attractor at the collision point. Using these kneading orbits, we can determine the collisions of a point of the unstable orbit with the chaotic attractor. Proceeding in this way for all orbits $O_{\mathcal{LR}^n}$ we get the boundaries of all large

triangular regions of the bandcount-increment scenario:

$$\gamma^{\ell}_{\mathcal{LR}^n} = \left\{ (a,b,\mu) \mid |a| < 1, \ b < -1, \ \mu = -\frac{ab^n - ab^2 + b^2 - 1}{(ab^n - ab + b^2 - 1)b} \right\},$$

$$\gamma^{r}_{\mathcal{LR}^n} = \left\{ (a,b,\mu) \mid |a| < 1, \ b < -1, \right. \tag{8.1}$$

$$\left. \mu = -\frac{(b^{n+4} - b^{n+2})a^2 + (b^{n+2} - b^4 + b^2 - 1)a - b^2 + 1}{(b^{n+4} - b^{n+2})a^2 + (b^{n+3} - b^4 + b^2 - 1)a - b^3 + b} \right\}.$$

These two sets of band-merging crisis surfaces give us the upper and lower boundaries of the large triangular regions. The remaining right vertical boundaries are given by the stability boundaries of the adjacent periodic regions, so that the regions $Q^{n+3}_{\mathcal{LR}^n}$ are bordered by the boundaries $\theta^{-}_{\mathcal{LR}^{n-2}}$. These borders are labeled in Figure 13(b) for the triangular region $Q^{8}_{\mathcal{LR}^5}$.

This describes the larger triangular regions, but the smaller regions shown in Figure 13 remain unexplained. Considering the lower boundaries of these regions, we see that they are induced by the same band-merging crises as the lower boundaries of the larger triangles. Therefore, we conclude that the above-mentioned smaller triangular regions are not really a separate phenomenon. In fact, they are part of the bigger triangles, which get overlapped by periodic regions. So the boundaries of the smaller regions consist entirely of already known bifurcation surfaces. A smaller region induced by the orbit $O^{u}_{\mathcal{LR}^n}$ has a lower boundary $\gamma^{r}_{\mathcal{LR}^n}$, a right boundary $\gamma^{\ell}_{\mathcal{LR}^{n+2}}$ (which are both band-merging crisis surfaces) and an upper boundary $\xi^{0,\ell}_{\mathcal{LR}^{n-2}}$ (which is a border collision surface). This is also shown in Figure 13(b), with the smaller region $Q^{8}_{\mathcal{LR}^5}$ in the middle part of the image. Since the bandcount-increment scenario is formed completely by the triangular regions, we will refer to them as "bandcount-increment regions".

A bandcount-increment region, which is not overlapped completely by its adjacent periodic region consists simply of the bigger triangular part of the region connected to the smaller part. The region $Q^{12}_{\mathcal{LR}^9}$ shown in Figure 13(b) is an example for that.

If a bandcount-increment region is overlapped by its adjacent periodic region or not depends on the value of a. For increasing a, less regions will be overlapped and vice versa. It is possible for every bandcount-increment region to find feasible values of a, so that it gets overlapped, and feasible values of a, so that it does not get overlapped.

This concludes the description of the bandcount-increment scenario. However, the bandcount-increment region Q^{inc} is far more complex than that. Explaining all existing substructures is beyond the scope of this work. For this reason, further exploration of the bandcount-increment region is left for subsequent works.

9. Summary

In this work the question, whether the bandcount-increment and the bandcount-adding scenario in system (1.3) interact with each other, is answered. It is demonstrated that this is not the case by determining that both scenarios exist in their own regions of the parameter space, Q^{add} and Q^{inc}, separated by the one-band attractor region Q^1. This observation is then followed by a detailed descriptions of the complete bandcount-adding scenario and the

(a)

(b)
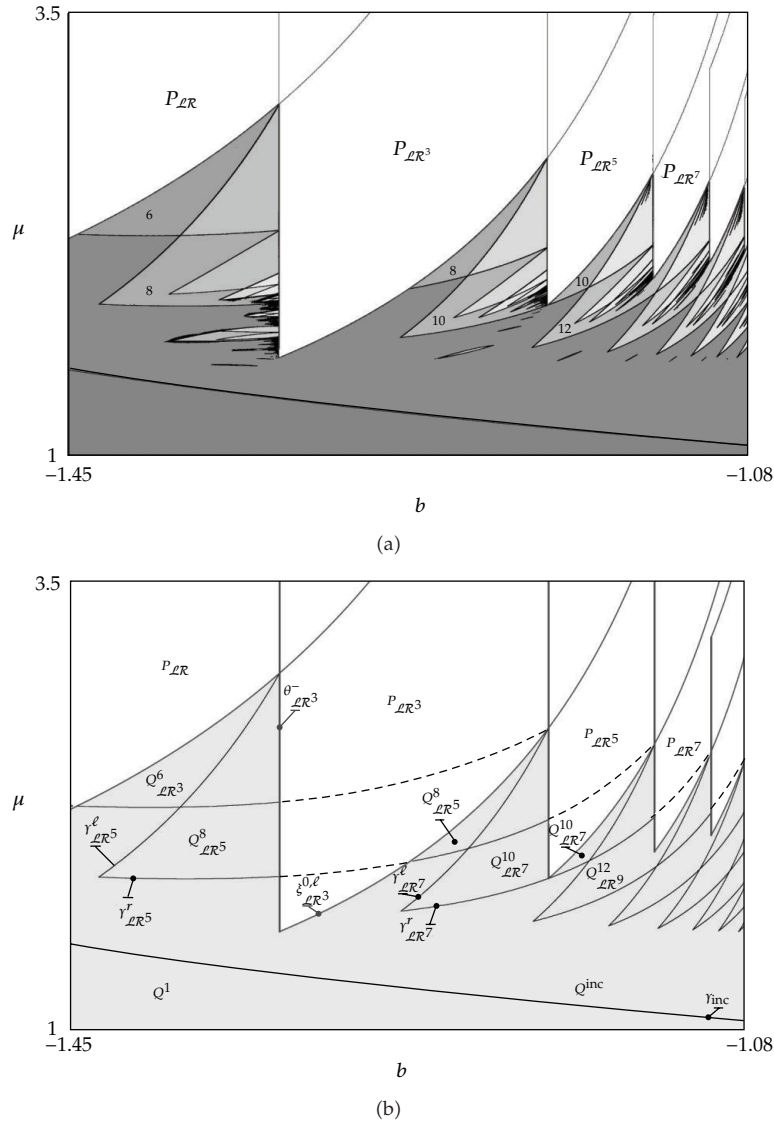
Figure 13: Parameter space diagram for $a = 0.42$, $b = -1.45 \cdots -1.08$, $\mu = 1.0 \cdots 3.5$. (a) shows the numerically determined bandcounts, while (b) shows the corresponding analytically determined diagram. In (a), regions are labeled with their bandcounts. The borders of two regions $Q^8_{\mathcal{LR}^5}$ are completely labeled, consisting of the band-merging crises $\gamma^\ell_{\mathcal{LR}^5}$ and $\gamma^r_{\mathcal{LR}^5}$, the stability border $\theta^-_{\mathcal{LR}^3}$ and the border collision $\xi^{0,\ell}_{\mathcal{LR}^3}$. Dotted lines show band-merging crisis curves inside periodic regions.

main structure of the bandcount-increment scenario. These descriptions confirm that no orbit involved in the bandcount-increment scenario influences the bandcount-adding scenario, and vice versa.

The descriptions of both scenarios also showed, that the bandcount-adding scenario in system (1.3) behaves exactly in the same way as it does in the previously investigated case (see [23]). However, for the bandcount-increment scenario the situation is more complicated. Although the main structure of the bandcount-increment scenario in system (1.3) is very
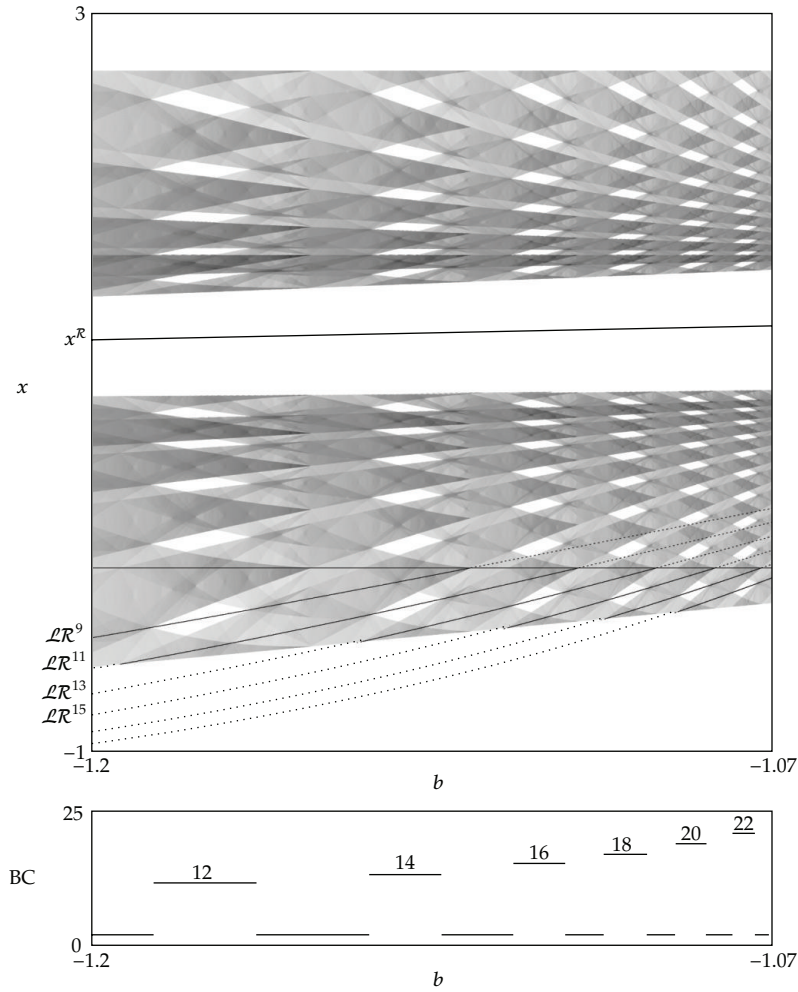
Figure 14: Bifurcation and bandcount diagrams for $a = 0.42$, $b = -1.2 \cdots -1.07$, $\mu = 1.7$. Each curve shows a single point of unstable periodic orbits of the form $O_{\mathcal{LR}^{2n+1}}$, each colliding with the attractor in two band-merging crises. Only one point per orbit is shown, for the sake of clarity, but the other points of the orbits also fit the gaps. Note that all orbits shown in this image, are destroyed in border collisions at $x = 0$. Their virtual parts are shown dashed. The location of this scenario in the (b, μ)-plane is marked with B in Figure 4(a).

similar to the previously investigated case (see [20–22]) there are remarkable differences especially with respect to the substructures. The investigation of these substructures is intricate and beyond the scope of this paper and is therefore left for future work.

List of Symbols

$\mathcal{L}/\mathcal{R}$: Symbols corresponding to points of a periodic orbit smaller/larger than 0, respectively

O_σ: Periodic orbit corresponding to a symbolic sequence σ

x_k^σ: The kth point of a periodic orbit O_σ

Q^{ch}:   The chaotic domain

Q^{add}:   The part of the chaotic domain organized by the bandcount-adding scenario

Q^{inc}:   The part of the chaotic domain organized by the bandcount-increment scenario

Q^1:   The part of the chaotic domain containing only a one-band attractor

Q_σ^k: A region in the chaotic domain with bandcount k, which is bounded by crisis bifurcations caused by the collision of the orbit O_σ with the chaotic attractor

$x_{c\cdots ba}^{ko}$:   A point of a kneading orbit corresponding to the sequence of iteration $f_a \circ f_b \circ \cdots \circ f_c(0)$, with $a, b, c \in \{r/\ell\}$

$\Omega(B)$:   The 3D influence region of the codimension-3 big bang bifurcation point B (see Section 3)

$\mathcal{M}^{\text{2D}}(B)$:   The 2D manifold of the codimension-3 big bang bifurcation point B (see Section 3)

$\mathcal{M}^{\text{1D}}(B)$:   The 1D manifold of the codimension-3 big bang bifurcation point B (see Section 3)

$\Omega^{\text{add}}(B)$:   The part of the influence region $\Omega(B)$ which is organized by the period adding scenario (see Section 3)

$\Omega^{\text{inc}}(B)$:   The part of the influence region $\Omega(B)$ which is organized by the period increment scenario (see Section 3)

τ^∞:   The boundary between $\mathcal{M}^{\text{2D}}(B_1)$ and $\mathcal{M}^{\text{2D}}(B_2)$ (see (4.1))

P: The parameter space region investigated in this work (see (3.2))

P_σ: A parameter space region in which the periodic orbit O_σ exists

P_σ^s: A subset of P_σ in which the periodic orbit O_σ is stable

$\xi_\sigma^{k,d}$:   A border collision caused by the periodic orbit O_σ, in which the kth point of the orbit collides with the border from the left/right, with $d \in \{l, r\}$, respectively, (see (4.4))

θ_σ^-:   A boundary at which the orbit O_σ becomes unstable via the eigenvalue -1. The boundary is defined by (4.6) and is relevant for the period increment scenario with coexisting attractors

θ_σ^+:   A boundary at which the orbit O_σ becomes unstable via the eigenvalue $+1$. The boundary is defined by (4.6) and is relevant for the period adding scenario

τ^{env}:   The border between the region $\Omega^{\text{add}}(B_1)$ and the chaotic domain (see (4.7))

γ_{add}:   The band-merging crisis which separates the region Q^1 from the region Q^{add} (see (5.1))

γ_{inc}:   The band-merging crisis which separates the region Q^1 from the region Q^{inc} (see (5.2))

γ_σ^d: A band-merging crisis caused by the orbit O_σ, with $d \in \{l, r\}$ (see (6.1))

η_σ^d: An interior crisis caused by the orbit O_σ, with $d \in \{l, r\}$ (see (6.1))

$a_{\gamma_{\text{inc}}}^n$:   The value of a at which γ_{inc} intersects the lowest point of the stability region $P_{\mathcal{LR}^n}^s$ (see (5.4))

ζ_σ: A point in parameter space at which the boundaries of the bandcount-adding region corresponding to O_σ intersect the boundary surface τ^{env}, as well as many other bifurcation curves (see (7.1)).

Acknowledgment

References

[1] S. Banerjee and G. C. Verghese, *Nonlinear Phenomena in Power Electronics: Attractors, Bifurcations, Chaos, and Nonlinear Control*, IEEE Press, 2001.

[2] Z. T. Zhusubaliyev and E. Mosekilde, *Bifurcations and Chaos in Piecewise-Smooth Dynamical Systems*, vol. 44 of *World Scientific Series on Nonlinear Science. Series A: Monographs and Treatises*, World Scientific, River Edge, NJ, USA, 2003.

[3] M. di Bernardo, C. J. Budd, A. R. Champneys, and P. Kowalczyk, *Piecewise-Smooth Dynamical Systems: Theory and Applications*, vol. 163 of *Applied Mathematical Sciences*, Springer, 2008.

[4] D. J. W. Simpson, *Bifurcations in Piecewise-Smooth Continuous Systems*, vol. 70 of *Nonlinear Science A*, World Scientific, 2010.

[5] M. Mita, M. Arai, S. Tensaka, D. Kobayashi, and H. Fujita, "A micromachined impact microactuator driven by electrostatic force," *Journal of Microelectromechanical Systems*, vol. 12, no. 1, pp. 37–41, 2003.

[6] X. Zhao, H. Dankowicz, C. K. Reddy, and A. H. Nayfeh, "Modeling and simulation methodology for impact microactuators," *Journal of Micromechanics and Microengineering*, vol. 14, no. 6, pp. 775–784, 2004.

[7] G. Karner, "The simplified Fermi accelerator in classical and quantum mechanics," *Journal of Statistical Physics*, vol. 77, no. 3-4, pp. 867–879, 1994.

[8] F. Saif, I. Bialynicki-Birula, M. Fortunato, and W. P. Schleich, "Fermi accelerator in atom optics," *Physical Review A*, vol. 58, no. 6, pp. 4779–4783, 1998.

[9] E. D. Leonel and P. V. E. McClintock, "Dissipative area-preserving one-dimensional Fermi accelerator model," *Physical Review E*, vol. 73, no. 6, Article ID 066223, 2006.

[10] E. Fermi, "On the origin of the cosmic radiation," *Physical Review*, vol. 75, no. 8, pp. 1169–1174, 1949.

[11] A. B. Nordmark, "Non-periodic motion caused by grazing incidence in an impact oscillator," *Journal of Sound and Vibration*, vol. 145, no. 2, pp. 279–297, 1991.

[12] A. B. Nordmark, "Universal limit mapping in grazing bifurcations," *Physical Review E*, vol. 55, no. 1, pp. 266–270, 1997.

[13] J. Molenaar, J. G. de Weger, and W. van de Water, "Mappings of grazing-impact oscillators," *Nonlinearity*, vol. 14, no. 2, pp. 301–321, 2001.

[14] P. Jain and S. Banerjee, "Border-collision bifurcations in one-dimensional discontinuous maps," *International Journal of Bifurcation and Chaos*, vol. 13, no. 11, pp. 3341–3351, 2003.

[15] H. E. Nusse and J. A. Yorke, "Border-collision bifurcations including "period two to period three" for piecewise smooth systems," *Physica D*, vol. 57, no. 1-2, pp. 39–57, 1992.

[16] H. E. Nusse and J. A. Yorke, "Border-collision bifurcations for piecewise smooth one-dimensional maps," *International Journal of Bifurcation and Chaos*, vol. 5, no. 1, pp. 189–207, 1995.

[17] V. Avrutin, M. Schanz, and S. Banerjee, "Codimension-three bifurcations: explanation of the complex one-,two-, and three-dimensional bifurcation structures in nonsmooth maps," *Physical Review E*, vol. 75, no. 6, Article ID 066205, 7 pages, 2007.

[18] Yu. L. Maistrenko, V. L. Maistrenko, and S. I. Vikul, "Bifurcations of attracting cycles of piecewise linear interval maps," *Journal of Technical Physics*, vol. 37, no. 3-4, pp. 367–370, 1996.

[19] Yu. L. Maistrenko, V. L. Maistrenko, and S. I. Vikul, "On period-adding sequences of attracting cycles in piecewise linear maps," *Chaos, Solitons & Fractals*, vol. 9, no. 1-2, pp. 67–75, 1998.

[20] V. Avrutin, B. Eckstein, and M. Schanz, "The bandcount increment scenario. I. Basic structures," *Proceedings of The Royal Society of London. Series A*, vol. 464, no. 2095, pp. 1867–1883, 2008.

[21] V. Avrutin, B. Eckstein, and M. Schanz, "The bandcount increment scenario. II. Interior structures," *Proceedings of The Royal Society of London. Series A*, vol. 464, no. 2097, pp. 2247–2263, 2008.

[22] V. Avrutin, B. Eckstein, and M. Schanz, "The bandcount increment scenario. III. Deformed structures," *Proceedings of The Royal Society of London. Series A*, vol. 465, no. 2101, pp. 41–57, 2009.

[23] V. Avrutin and M. Schanz, "On the fully developed bandcount adding scenario," *Nonlinearity*, vol. 21, no. 5, pp. 1077–1103, 2008.

[24] V. Avrutin, M. Schanz, and S. Banerjee, "Multi-parametric bifurcations in a piecewise-linear discontinuous map," *Nonlinearity*, vol. 19, no. 8, pp. 1875–1906, 2006.

[25] S. Banerjee, J. A. Yorke, and C. Grebogi, "Robust chaos," *Physical Review Letters*, vol. 80, no. 14, pp. 3049–3052, 1998.

[26] C. Mira, "Détermination pratique du domaine de stabilité d'un point d'équilibre d'une récurrence non linéaire du deuxième ordre à variable réelle," *Comptes Rendus de l'Académie des Sciences*, vol. 261-262, pp. 5314–5317, 1964.

[27] C. Mira, "Determination graphique de la frontiére de stabilité dun point d'équilibre dune récurrence nonlinéaire du deuxiéme ordre à variables réelles-application au cas où les seconds membres de la récurrence ne sont pas analytiques," *Comptes Rendus de l'Académie des Sciences*, vol. 262, pp. 951–954, 1966.

[28] I. Gumowski and C. Mira, "Solutions "chaotiques" bornées d'une récurrence, ou transformation ponctuelle du deuxième ordre, à inverse non unique," *Comptes Rendus de l'Académie des Sciences. Séries A*, vol. 285, no. 6, pp. A477–A480, 1977.

[29] I. Gumowski and C. Mira, "Bifurcation déstabilisant une solution chaotique d'un endomorphisme du deuxième ordre," *Comptes Rendus de l'Académie des Sciences. Séries A*, vol. 286, no. 9, pp. A427–A430, 1978.

[30] I. Gumowski and C. Mira, *Dynamique Chaotique, Transformations Ponctuelles. Transition. Ordre-Désordre*, Cepadues Éditions, Toulouse, France, 1980.

[31] C. Grebogi, E. Ott, and J. A. Yorke, "Chaotic attractors in crisis," *Physical Review Letters*, vol. 48, no. 22, pp. 1507–1510, 1982.

[32] C. Grebogi, E. Ott, and J. A. Yorke, "Crises, sudden changes in chaotic attractors, and transient chaos," *Physica D*, vol. 7, no. 1-3, pp. 181–200, 1983.

[33] D. Stynes and D. M. Heffernan, "Universality and scaling in chaotic attractor-to-chaotic attractor transitions," *Chaos, Solitons & Fractals*, vol. 13, no. 6, pp. 1195–1204, 2002.

[34] S. H. C. Marcos, S. R. Lopes, and R. L. Viana, "Boundary crises, fractal basin boundaries, and electric power collapses," *Chaos, Solitons & Fractals*, vol. 15, no. 2, pp. 417–424, 2003.

[35] F. A. Borotto, A. C.-L. Chian, T. Hada, and E. L. Rempel, "Chaos in driven Alfvén systems: boundary and interior crises," *Physica D*, vol. 194, no. 3-4, pp. 275–282, 2004.

[36] A. C. L. Chian, F. A. Borotto, E. L. Rempel, and C. Rogers, "Attractor merging crisis in chaotic business cycles," *Chaos, Solitons & Fractals*, vol. 24, no. 3, pp. 869–875, 2005.

[37] A. C.-L. Chian, E. L. Rempel, and C. Rogers, "Complex economic dynamics: chaotic saddle, crisis and intermittency," *Chaos, Solitons & Fractals*, vol. 29, no. 5, pp. 1194–1218, 2006.

[38] Q. Bi, "Chaos crisis in coupled Duffing's systems with initial phase difference," *Physics Letters A*, vol. 369, no. 5-6, pp. 418–431, 2007.

[39] B. L. Hao, *Elementary Symbolic Dynamics and Chaos in Dissipative Systems*, World Scientific, Teaneck, NJ, USA, 1989.

[40] C. Mira, L. Gardini, A. Barugola, and J.-C. Cathala, *Chaotic Dynamics in Two-Dimensional Noninvertible Maps*, vol. 20 of *World Scientific Series on Nonlinear Science. Series A: Monographs and Treatises*, World Scientific, River Edge, NJ, USA, 1996.

[41] V. Avrutin and M. Schanz, "On multi-parametric bifurcations in a scalar piecewise-linear map," *Nonlinearity*, vol. 19, no. 3, pp. 531–552, 2006.

[42] J. Farey, "On a curious property of vulgar fractions," *The Philosophical Magazine and Journal*, vol. 4, pp. 385–386, 1816.

[43] J. C. Lagarias and C. P. Tresser, "A walk along the branches of the extended Farey tree," *IBM Journal of Research and Development*, vol. 39, no. 3, pp. 283–294, 1995.

[44] M. A. Stern, "Über eine zahlentheoretische Funktion," *Journal für die reine und angewandte Mathematik*, vol. 55, pp. 183–220, 1858.

[45] A. Brocot, "Calcul des rouages par approximation, nouvelle méthode," *Revue Chronometrique*, vol. 3, pp. 186–194, 1861.

[46] I. Sushko and L. Gardini, "Degenerate bifurcations and border collisions in piecewise smooth 1D and 2D maps," *International Journal of Bifurcation and Chaos*, vol. 20, no. 7, pp. 2045–2070, 2010.

[47] L. Gardini, F. Tramontana, V. Avrutin, and M. Schanz, "Border-collision bifurcations in 1D piecewise-linear maps and Leonov's approach," *International Journal of Bifurcation and Chaos*, vol. 20, no. 10, pp. 3085–3104, 2010.

[48] V. Avrutin, B. Eckstein, and M. Schanz, "On detection of multi-band chaotic attractors," *Proceedings of The Royal Society of London. Series A*, vol. 463, no. 2081, pp. 1339–1358, 2007.